ANALYSIS OF STIMULATED RAMAN SCATTERING ON THE PERFORMANCE OF AN OPTICAL WAVELENGTH DIVISION MULTIPLEXED SYSTEM

by

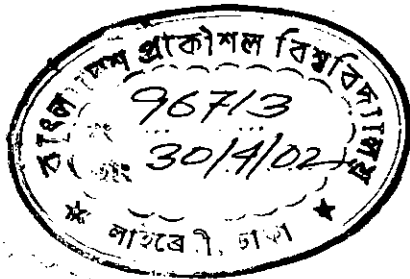## Md. Golam Mostafa

A thesis submitted in partial fulfillment of the requirements for the degree of

MASTER OF SCIENCE

IN

ELECTRICAL AND ELECTRONIC ENGINEERING

Department of Electrical and Electronic Engineering

BANGLADESH UNIVERSITY OF ENGINEERING AND TECHNOLOGY

2002

March 30, 2002

APPROVAL CERTIFICATE

The thesis titled "Analysis of stimulated Raman scattering on the performance of an optical wavelength division multiplexed system" by Md. Golam Mostafa, Student No. 040006235F of April 2000 session, is hereby approved and recommended for acceptance for the degree of Master of Science in Engineering (Electrical and Electronic).
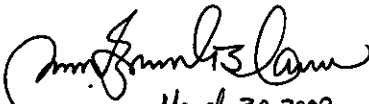
BOARD OF EXAMINERS

1. **Chairman (Supervisor):**
   Dr. M. Nazrul Islam
   Assistant Professor
   Dept. of Electrical and Electronic Engineering
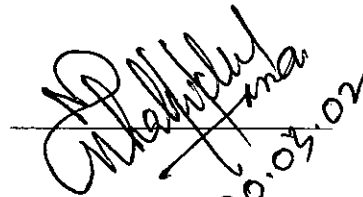   BUET, Dhaka 1000.

   March 30, 2002

2. **Member (Ex-Officio):**
   Dr. M. M. Shahidul Hassan
   Professor and Head
   Dept. of Electrical and Electronic Engineering
   BUET, Dhaka 1000.

3. **Member:**
   Dr. Md. Saifur Rahman
   Professor
   Dept. of Electrical and Electronic Engineering
   BUET, Dhaka 1000.

   30.03.02

4. **Member:**
   Dr. Md. Shah Alam
   Assistant Professor
   Dept. of Electrical and Electronic Engineering
   BUET, Dhaka 1000.

   30.3.02

5. **Member (External):**
   Dr. Md. Faruk Ahmed
   Professor
   Dept. of Applied Physics and Electronics
   Dhaka University, Dhaka 1000.

   30.3, 2002

March 30, 2002

DECLARATION

It is hereby declared that this thesis or any part of it has not been submitted elsewhere for the award of any degree or diploma.
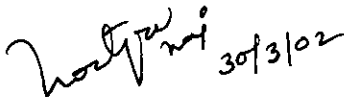
Signature of the supervisor

March 30, 2002

Dr. M. Nazrul Islam
Assistant Professor
Dept. of Electrical and Electronic Engineering
BUET, Dhaka

Signature of the candidate

30/3/02

Md. Golam Mostafa

Dedicated to my beloved parents,
Md Ahakamul Hoque
And
Begum Sabira Hoque

TABLE OF CONTENTS

Chapter 3: Performance of Wideband WDM System

Chapter 4: Statistical Analysis of Raman Crosstalk

Chapter 5: Conclusions

LIST OF FIGURES

LIST OF SYMBOLS

γ	SRS gain coefficient
α	attenuation constant of fiber
η	mean value of depletion
λ	wavelength
$\Delta\lambda$	channel separation in wavelength
$\Delta\nu$	channel separation in frequency
σ^2	variance of depletion
γ_p	peak Raman gain coefficient
A_{eff}	effective core area
b	polarization factor
D	fractional lost power or depletion
g	gain coefficient
I_{th}	threshold level of the decision circuit at the receiver
L	fiber length
L_{eff}	effective fiber length

m_i ·   modulation index in the ith channel

N number of channels

P_0 power launched at the input of a fiber

$P_1(0)$ power of the wave entering the medium of length L.

$P_1(L)$ power of the wave exiting the medium of length L.

P_2 power of the pump wave

P_{crit} critical power

P_D probability of having a depletion D

P_e bit error rate or probability of error

$P_{e|0}$ probability of error when a "0" has been transmitted

$P_{e|1}$ probability of error when a "1" has been transmitted

P_T transmitted power

X power penalty

LIST OF ABBREVIATIONS

APD	Avalanche Photo Diode
ASK	Amplitude Shift Keying
BER	Bit Error Rate
BPPM	Binary Pulse Position Modulation
BPSK	Binary Phase Shift Keying
CPFSK	Continuous Phase Frequency Shift Keying
dB	deciBel
DD	Direct Detection
DPFSK	Discontinuous Phase Frequency Shift Keying
DPSK	Differential Phase Shift Keying
DSF	Dispersion Shifted Fiber
DWDM	Dense Wavelength Division Multiplexing
EMI	ElectroMagnetic Interference
EMP	ElectroMagnetic Pulses
FDM	Frequency Division Multiplexing
FSK	Frequency Shift Keying
GHz	GigaHertz
GVD	Group Velocity Dispersion
IF	Intermediate Frequency
IM	Intensity Modulation
ISDN	Integrated Service Digital Networks
ISI	Inter Symbol Interference
LASER	Light Amplification by Stimulated Emission of Radiation
LD	Laser Diode
LED	Light Emitting Diode
LO	Local Oscillator

MHz	MegaHertz
OFDM	Optic/Orthogonal Frequency Division Multiplexing
OQPSK	Orthogonal Quadrature Phase Shift Keying
PDF	Probability Density Function
PIN	Positive-Intrinsic-Negative
PSK	Phase Shift Keying
QPSK	Quadrature Phase Shift Keying
RFI	Radio Frequency Interference
SBS	Stimulated Brillouin Scattering
SDH	Synchronous Digital Hierarchy
SLD	Semiconductor Laser Diode
SMF	Single-Mode Fiber
SONET	Synchronous Optical Network
SPM	Self Phase Modulation
SRS	Stimulated Raman Scattering
THz	TeraHertz
WDM	Wavelength Division Multiplexing
XPM	Cross Phase Modulation.

ACKNOWLEDGMENTS

ABSTRACT

Wavelength-division multiplexing (WDM) technology effectively utilizes the enormous bandwidth of an optical fiber by multiplexing numerous channels at different wavelengths. However, a high power WDM system suffers performance degradation due to several nonlinear interactions between the information bearing lightwaves and the transmission medium. These optical nonlinearities can lead to interference, distortion and excess attenuation of optical signals. Among the nonlinear effects, stimulated Raman scattering (SRS) is found to be the ultimate power-limiting phenomenon for a wide band WDM system. The SRS effect causes frequency conversion of light and results in excess attenuation of short-wavelength channels in wavelength-multiplexed systems, and thus induces interchannel modulation between each WDM channel. The analysis shows that the product of total power and total bandwidth must be smaller than 500 GHz-W to reduce the degradation due to SRS to an acceptable level.

In all the analyses of the Raman crosstalk reported so far, the experimentally found Raman gain profile of silica is approximated by a triangular function, where the peak Raman gain occurs at 15 THz spacing between channels and no Raman gain is assumed at larger spacing. However, for a wide-band WDM system, this approximate model of the Raman gain becomes insufficient to depict the system limitations. Therefore, an improved model is proposed for the Raman gain profile of silica, which includes, in addition to the linearly increasing function assumed in previous works, a linearly decreasing function and an exponentially decreasing function to approximate the tail of the Raman gain profile. The model is used to calculate the power depletion of the shortest-wavelength channel

due to the SRS effects from all other channels in a wide-band WDM system. The channels are considered to be equally spaced. Expression for power depletion and the power penalty suffered by the system due to SRS crosstalk is evaluated. Based on this improved model, the performance analysis of a WDM system is modified and generalized.

The probability density function (PDF) of the Raman crosstalk is approximated by a Gaussian distribution. Thus the probability of error due to SRS crosstalk is evaluated. A statistical analysis of the WDM system performance is developed to estimate the system bit error rate, which in turn is used to estimate the power penalty suffered by the system. Finally, the system limitations for a given maximum penalty are quantified.

Chapter 1

INTRODUCTION
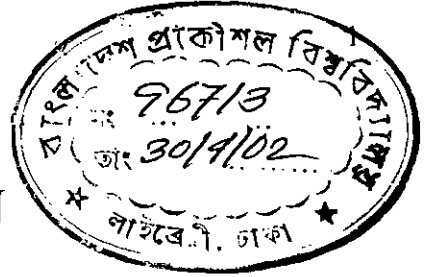
1.1 Overview of Optical Communication

History of optical communication dates back to the ancient age. The early civilizations used smoke signals, reflected sunlight, fire beacon and more recently, signaling lamps for limited but successful information transfer. In 1880 Alexander Graham Bell reported the transmission of speech using a light beam [Bell, 1880]. The photophone was proposed by Bell just four years after the invention of telephone. It allowed speech transmission over a distance of 200 m by modulated sunlight with a diaphragm. In modern communication system, with the increment of carrier frequency the transmission bandwidth increases theoretically, which in turn increases the information capacity of the channel. In subsequent years research interests have been grown to utilize an increasingly larger portion of the electromagnetic (EM) spectrum (EM spectrum is shown in Fig. 1.1) for conveying information. Thus with the human's earlier fascination in light, the recent trends of exploiting EM spectrum give the visible and infrared spectrum a significant position in communication engineering.

The basic principles of total internal reflection, responsible for guiding of light in optical fibers, were known from the nineteenth century. Although uncladded glass fibers were fabricated in the 1920s, the field of fiber optics was not born until the 1950s when the use of

a cladding layer led to a considerable improvement in the fiber characteristics. The invention of LASER in 1960s stimulated a renewed interest in the field of optical communication [Kao, 1966]. Since then, the research and development activities continued with the objectives of lowering the attenuation and widening the usage of wavelength range.
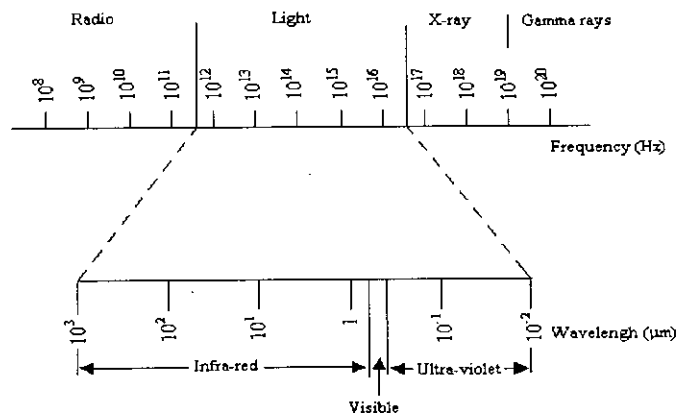
Fig. 1.1: Spectrum of electromagnetic waves.

The early uncladded glass fibers were extremely lossy (typical loss~1000 dB/km) from the modern standard. However, the situation changed drastically in 1970 when the loss of silica fiber was reduced to about 20 dB/km [Kapron, 1970]. By 1979, further progress in the fabrication technology resulted in a loss of about 0.2 dB/km near the 1.55μm wavelength [Miya, 1979], a loss level limited mainly by the fundamental process of Rayleigh scattering. By 1980s, these activities had led to the development and worldwide installation of practical and commercially feasible optical fiber communication systems that can carry telephone, cable television, data and other telecommunication traffics.

The present trend is such that in the near future optical fiber communications will be the heart of information and communication technology all over the world. The explosive growth of Internet traffic provides strong incentives to exploit the huge bandwidth of fiber optic networks. Such requirements are presently met by synchronous network technology (SONET/SDH) and are most likely to be met in the near future by ideally suited wavelength-division multiplexing (WDM) and its improved version, dense wavelength-division multiplexing (DWDM) technology. In a decade or two, when the total silica based fiber will be replaced by fiber made up with photonic band gap material or even with any other improved material, the communication system will overcome its limitations imposed by the properties of todays fiber. In addition to advanced in fiber technology, coherent source (e.g., LASER) and detector technology, amplification, modulation and switching, especially in an all-optical domain, the optical fiber communication system would become more attractive.

The attractive features of optical fiber communications are as follows:

- Enormous potential bandwidth (~50 THz),

- Small size and weight (~human hair),

- Electrical isolation (no earth loop, arcing, spark hazard),

- Immunity to interference and crosstalk (EMI, RFI, EMP, fiber to fiber interference),

- Signal security (optical signal does not radiate, so it cannot be accessed in a noninvasive manner),

- Low transmission loss (~0.2 dB/km, wide repeater spacing),

- Ruggedness and flexibility (high tensile strength, compact, can be twisted or bent, durable),

- System reliability and ease of maintenance (requires less repeaters; optical components are also reliable and requires less maintenance),

- Potential low cost.

1.2 The General Optical Communication System

The basic idea of a communication system is shown in Fig. 1.2 [Kieser, 1983]. The transmitter manipulates the information from message source and couples it onto a transmission channel in the form of signal, which matches the transfer properties of the channel. The channel bridges the distance between the transmitter and the receiver. All signals propagating through the channel become attenuated and distorted due to variations in channel properties and also due to interference. However, the receiver extracts the weakened and distorted signal from the channel, amplifies it and restores it to the original form, and passes it to the desired destination.

The block diagram of an optical communication system is shown in Fig. 1.3. The main components are:

- Optical source,

- Optical modulator,

- Optical fiber as a transmission wave guide,

- Optical detector,

- Demodulator.

In an optical communication system electrical signals are first converted into optical signals by modulating an optical source. Then the optical signal is launched into the fiber and is transmitted over a long distance. At the receiving end, the optical signal is converted into electrical signal by a photodetector followed by a demodulator.

Two conventional light sources are used in optical fiber communication, they are:

- Light emitting diodes (LED),

- Laser Diode (LD).

The advantages of an LED are:

(i)   less sensitive to retro reflection,

(ii)   possesses no interference problem,

(iii)   less sensitive to temperature variation,

(iv)   high reliability,

(v)   simple electronic excitation,

(vi)   less costly.
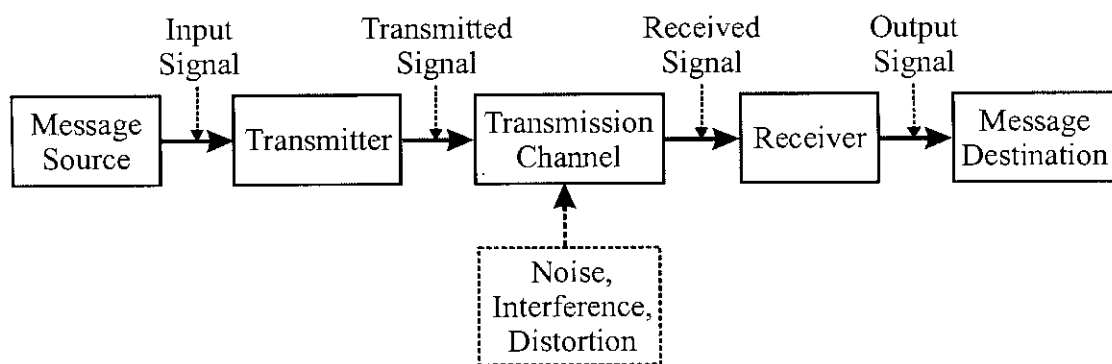
Fig. 1.2: Fundamental elements of a communication system
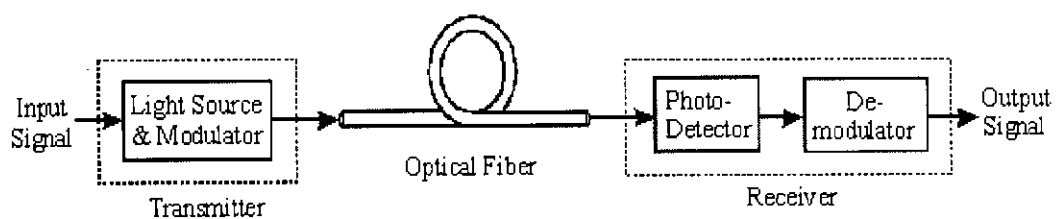
Fig. 1.3: Basic configuration of an optical communication system.

However, the LED has its disadvantages as well. The main disadvantages are:

(i)   low coupling efficiency between an LED and a fiber,

(ii)   low modulation bandwidth, typically limited to 100 MHz to 200 MHz,

(iii) wide spectral width of about 50-100 MHz around 50 nm.

The advantages of an LD are:

(i)   high conservation gain i.e. with small bias current relatively high power output,

(ii)   low numerical aperture and as a result a high coupling efficiency,

(iii) high modulation bandwidth,

(iv)   narrow spectral width (10-50 MHz).

The main disadvantages of an LD are:

(i)   highly sensitive to temperature variation,

(ii)   produce supplementary to return reflected power,

(iii) less reliable,

(iv)   more costly.

It is worth noting here that the LED is suitable for short links (<10 km), whereas the LD is suitable for medium and long links.

Two types of photodetectors are used in an optical fiber communication system, namely,

- positive-intrinsic-negative (PIN) photodiode,

- avalanche photodiode (APD).

For short links Ge PIN is used. For medium links Ge III/V PIN or Ge APD is used and for long links III/V APD is used.

After optical signal has been launched into the fiber, it becomes progressively attenuated and distorted with the increasing distance because of scattering, absorption, and dispersion in the fiber. At the receiver the attenuated and distorted optical power is detected by the photodiode. The figure of merit for a fiber is the attenuation and distortion which should be minimum and for a receiver there is a minimum optical power necessary at the desired data rate to attain either a given error probability for a digital system or a specified signal to noise ratio for an analog system.

In optical communication systems, two important detection techniques are normally employed. These are:

- direct detection,

- coherent detection.

In direct detection, a photodetector only respond to changes in the power level (the intensity) of an optical signal and not to its frequency and phase content. This is why it is known as intensity modulation direct detection (IM/DD). The IM/DD systems are simple and less costly but they suffer from limited sensitivity and do not take full advantage of the
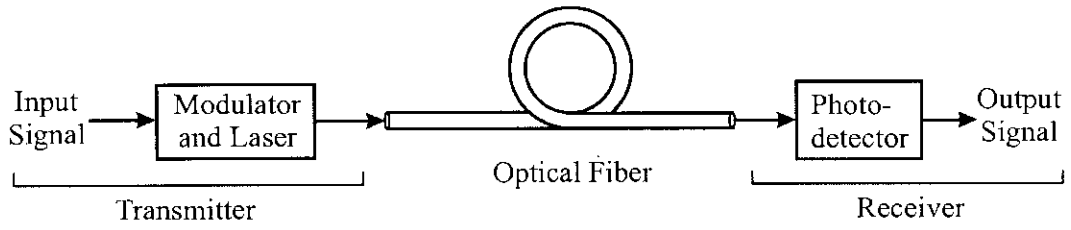
Fig. 1.4: Configuration of an IM-DD optical communication system
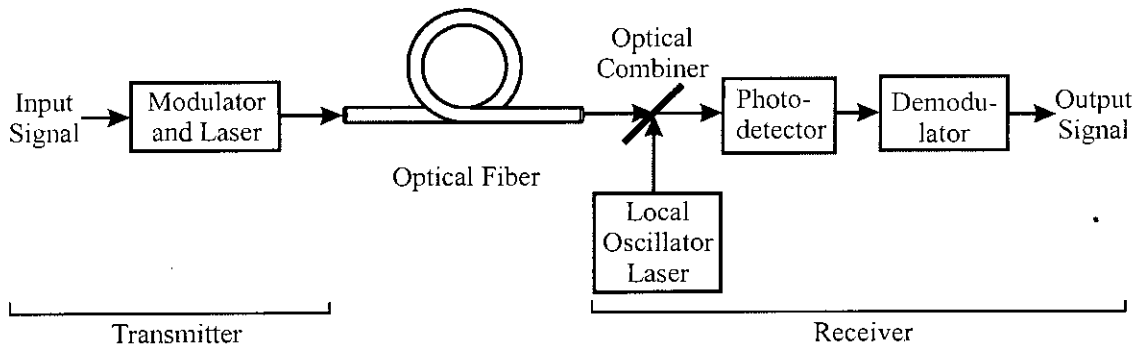
Fig. 1.5: Configuration of a coherent optical communication system

tremendous bandwidth capabilities of optical fiber due to relatively low optical power output of semiconductor laser diode (SLD). Direct detection optical communication systems were found very promising for future deep space applications, inter-satellite links and terrestrial line of sight communications. To increase the data rate throughput of all semiconductor free space optical channels, extensive research on bandwidth increase, power efficient coding and modulation schemes were carried out in the last decade.

Coherent light wave communication systems use a local oscillator (LO) to convert the received optical signal to an intermediate frequency (IF) signal (heterodyne system) or a baseband signal (homodyne system). Coherent systems are becoming more attractive for long haul transmission and wide band data distribution. Two major advantages that coherent systems offer are:

(i)   improved receiver sensitivity (up to 20 dB) relative to direct detection so that either the bit rate or the repeater spacing can be greatly increased,

(ii)   a high degree of frequency selectivity.

In coherent communication system, information can be impressed on the optical carrier using one of the three digital modulation schemes,

(i)   phase shift keying (PSK),

(ii)   frequency shift keying (FSK),

(iii)   amplitude shift keying (ASK)

Depending on the specific application various modulation and demodulation formats, similar to those of traditional radio frequency communications, are also employed in coherent light wave transmission. These include: binary PSK (BPSK), quadrature PSK (QPSK), orthogonal QPSK (OQPSK), continuous phase FSK (CPFSK), discontinuous phase FSK (DPFSK), binary pulse position modulation (BPPM) etc. Each of the modulation schemes and combinations thereof, with homodyne, heterodyne or diversity receivers has its own merits and demerits and none has emerged as absolutely preferable.

1.3 Multichannel Optical System

The huge transmission capacity of single mode fibers can be exploited efficiently by accessing the fiber bandwidth in the wavelength domain rather than in the time domain. The development of optical communication systems from the past can be viewed in terms of evolution through three generations of technology [Henry, 1985]. The first generation optical communication systems utilized multi-mode fiber having a core diameter of around 50 μm and the laser sources radiated in the so-called first transmission window, a wavelength of about 0.85 μm which is defined in Fig. 1.6. The second generation systems used mostly single-mode fibers and longer source wavelengths of 1.3 μm. The third generation utilizes a still longer wavelength of 1.55 μm where the attenuation of silica fibers is at a minimum, thereby achieving higher capacity and longer repeater spacing. Since the mid-1980s, the single-mode optical fiber systems have totally dominated high bandwidth overland and undersea telecommunications [Gowar, 1993]. The future generations may proceed further using longer wavelengths.

The information transfer rate can be maximized by fully utilizing the huge bandwidths available in the low-loss windows using multiplexing techniques. There are two techniques for this purpose, namely,

- Frequency Division Multiplexing (FDM),

- Wavelength Division Multiplexing (WDM).

The low-loss windows of optical fiber can be utilized best by optimizing two factors:

- information transfer rate,

- repeaterless distance.
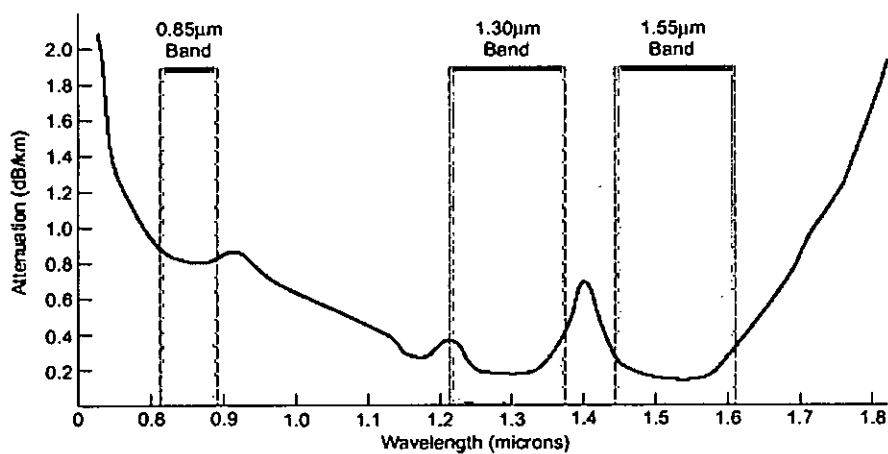
Fig. 1.6: Attenuation of light in silica fiber. Three filled columns indicate transmission windows used in optical fiber communication.

Both techniques are identical in the sense that optical power from more than one LASER travels through a single fiber. The difference is that the channel spacing for a WDM system is on the order of 0.1 μm, while for an FDM system it is on the order of 0.1 nm. For WDM

systems, demultiplexing can be done in the optical domain. However, coherent receivers are required for FDM systems, and the demultiplexing must be done in the electrical domain. For the best performance, narrow line width, stable, single-mode LASERs should be used for both WDM and FDM systems. The repeaterless transmission distance can be increased by

- increasing the sensitivity at the receiving end,

- increasing the launched power at the transmitter end.

The receiver sensitivity can be improved by using coherent receivers. Another advantage of using coherent receiver is that the frequency spacing between channels can be reduced to a minimum level, since the demultiplexing can be done in the electrical domain. On the other hand, high power LASERs are required to increase the repeaterless distance.

1.3.1 Frequency Division Multiplexing

FDM is a method of providing a number of simultaneous channels over a common transmission path by using a different frequency band for the transmission of each channel. A block diagram of a FDM system is shown in Fig. 1.7. As indicated in the figure, an FDM system divides the available bandwidth of the transmission medium into a number of narrower bands or sub channels. The individual signals can be extracted from the combined FDM signal by appropriate electrical filtering. Hence frequency division

multiplexing in IM/DD system is generally performed electrically in the transmit terminal prior to intensity modulation of a single optical source.

1.3.2 Wavelength Division Multiplexing (WDM)

Wavelength division multiplexing (WDM) involves the transmission of a number of different peak wavelength optical signals in parallel on a single optical fiber. The concept of WDM is illustrated in Fig. 1.8 showing the coupling of separate sources into a fiber and the separation of the signals out of the fiber.

Among WDM systems, dense WDM (DWDM), where the channel spacing is a few times the bit rate, allows the possibility of transmitting many channels simultaneously, increasing the transmission capacity. A sharp cutoff filter and a modulation scheme with compact spectrum are necessary to construct densely spaced multiplexing system using direct detection scheme.

Telecommunications make wide use of optical techniques where the carrier wave belongs to the classical optical domain. The wave modulation allows transmission of analog or digital signals up to a few gigahertz or gigabits per second on a carrier whose frequency is very high, typically 192 to 196 THz (infrared). In fact, using several carrier waves that are propagating without significant interaction on the same cable can increase the bit rate further.
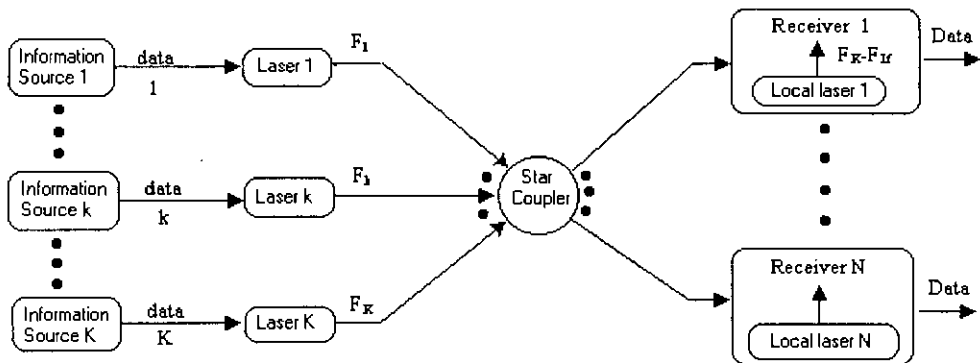
Fig. 1.7: Block diagram of FDM system
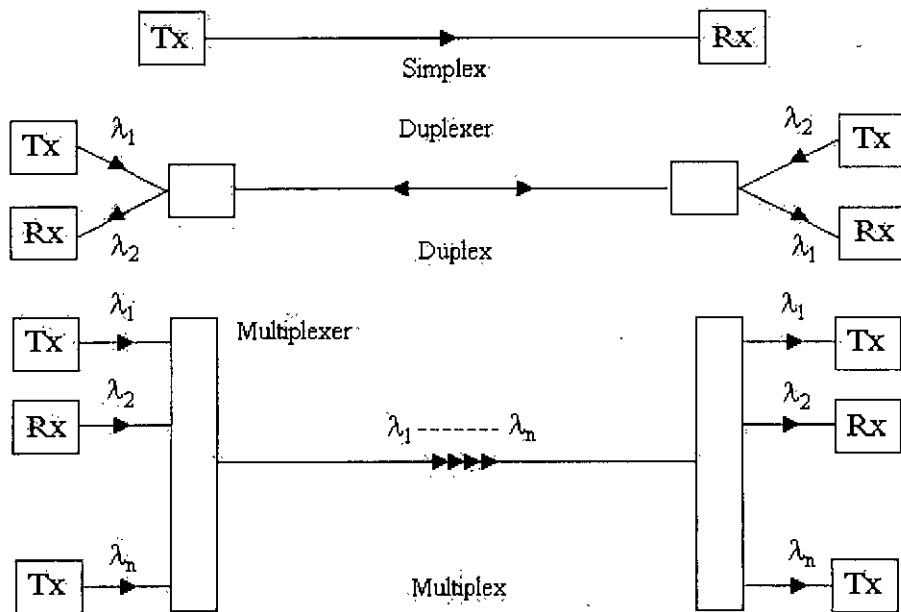
Fig. 1.8: Typical WDM transmission link.

With wavelength division multiplexing it is possible to couple sources emitting at different wavelengths. For the multiplexing (or separation) of wavelengths, interference filters or gratings can be used. However, wavelength division multiplexers using interference filters cannot be used when the number of channels is too high or when the wavelengths are too close. The main advantage of the grating is the simultaneous diffraction of all wavelengths and therefore, it is possible to construct simple devices with a very large number of channels (with the exception of fiber gratings). There are three types of gratings, namely,

- classical gratings,

- arrayed waveguide gratings,

- fiber gratings.

In the classical grating, we use gratings in the Stimax configuration as shown in Fig. 1.9. Grating multi/demultiplexers consists of three main parts: entrance and exit elements (fiber array or transmission line fiber, emitters or receivers) focusing optics and dispersive grating. The concave mirror transforms the diverging beam coming from any fiber into a parallel beam. The beam then hits grating and is angularly dispersed back to the concave mirror where it is imaged, depending on its wavelength, onto the output fiber array. The dispersive element was a grating embedded in a monoblock of silica, and the optical fibers were directly fixed to the block. The number of grooves on the grating (several tens to several thousands per millimeter) is obtained by using a diamond tool or by holographic photoetching. The grating has the property of diffracting light in a direction related to its wavelength as shown in Fig.1.10. Hence an incident beam with several wavelengths is angularly separated in different directions. Conversely, several wavelengths coming from
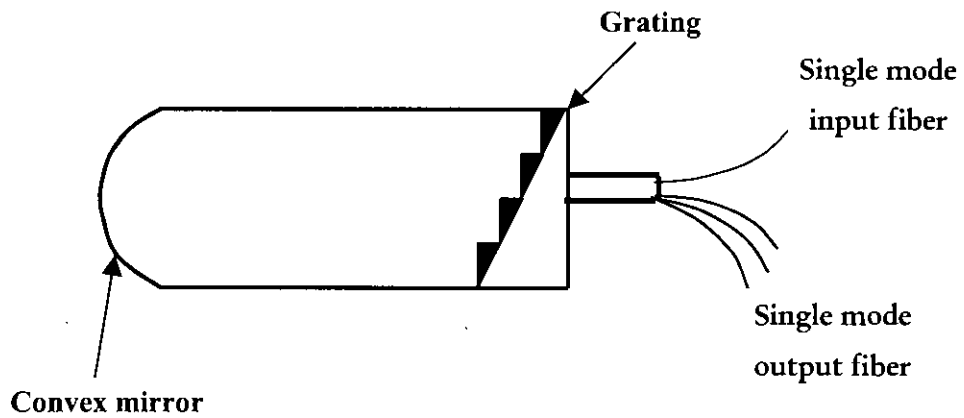
Fig. 1.9: Stimax configuration.
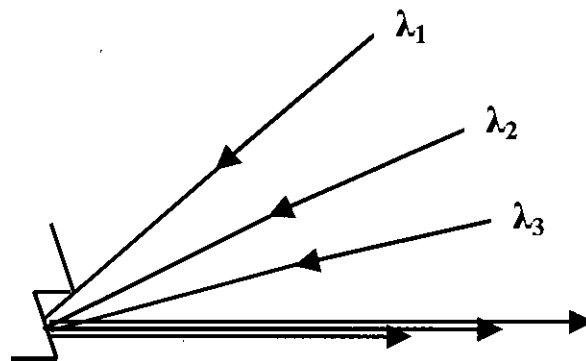
Fig. 1.10: Principle of multiplexing by diffraction on an optical grating. Wavelengths λ_1, λ_2 ... λ_n coming from different directions, are diffracted in the same direction into a single transmission line.

different directions can be combined in the same direction. The diffraction angle depends on the groove spacing and on the incidence angle.

The arrayed waveguide grating was designed to increase the resolving power, i.e., the fine splitting of the wavelengths. Using a waveguide structure equivalent to the well-known Michelson echelon gratings in classical optics increased the optical path difference between the diffracting elements. Such structure has the advantage of smaller channel spacing. Its disadvantages are (1) a much smaller free spectral range that will limit the total number of channels and (2) near-end crosstalk that affects bi-directionality.

Recording a Bragg grating in the core of single-mode fiber made photosensitive by doping with, for example, germanium makes a fiber grating. This grating can be used as a narrowband filter. It is necessary to use one grating per wavelength. So there is some limitation to the number of channels that can be obtained with these devices.

In order to get more channels at smaller wavelength spacing higher dispersion gratings is needed, which means more grooves per millimeter. Unfortunately, this generally means gratings with more crosstalk and a larger polarization rate.

There is indeed about 15,000 gigahertz of optical frequency bandwidth in each 1300-nm and 1550-nm window as shown in Fig. 1.6. With 5 gigabits per second bit rate, the uncertainty relationship gives about 5 gigahertz limit for optical frequency spacing (or about 100-nm optical wavelength bandwidth). This would mean 3000 channels! Each channel can be separated by 0.03 nm. In reality, the separation between channels is now 1 nm or a few nanometers on most of the installed networks using WDM, with each wavelength signal having a full-width-half maximum smaller than 0.03 nm.

An International Telecommunication Union standardization is currently underway that would propose a frequency grid with separations of 100 gigahertz (about 0.8 nm) with multiples and submultiples. Now, the published minimum channel spacing is about 0.1 nm. However, nothing lower than 0.4 nm (50 gigahertz) spacing is commercially available. These spacing are obtained on WDM using classical gratings (Stimax from Jobin Yvon, for example), arrayed waveguide gratings (Lucent, for example), or Bragg grating filters (3M).

Applications such as video networks linking workstations, television studio center signal routing systems, videoconference networks, interactive video training systems, bank information service networks and data transfer networks between computers, integrated services digital network (ISDN), tele-distribution, and generally all broadband networks increasingly use both time and wavelength multiplexed optical lines.

1.4 Limitations of Optical Fiber Communications

In spite of several advantages, the optical fiber communication system has its own limitations, which are as follows:

- Fiber attenuation,

- Dispersion,

- Nonlinear effects.

1.4.1 Fiber Attenuation

An important parameter of optical filter is the measure of power loss during transmission of optical signal inside the fiber. If P_0 is the power launched at the input of a fiber of length L, the transmitted power P_T is given by

$$P_T = P_0 \exp(-\alpha L) \tag{1.1}$$

where α is the attenuation constant, commonly referred as fiber loss.

It is customary to express the fiber loss in units of dB/km by using the relation

$$\alpha_{dB} = -\frac{10}{L} \log \frac{P_T}{P_0} = 4.343\alpha \tag{1.2}$$

The measured loss spectrum for an ultra-low-loss single mode fiber with the calculated attenuation spectra for some of the loss mechanism contributing the overall fiber attenuation (dashed and dotted lines) are shown in Fig. 1.11 [Miya, 1979]. The fiber exhibits a minimum loss of about 0.2 dB/km near 1.55 μm. The loss is considerably higher in shorter wavelengths, reaching a level of 1-10 dB/km in the visible region. It is to be noted that even a 10 dB/km loss corresponds to an attenuation constant of only $\alpha \approx 2 \times 10^{-5}$ cm^{-1}, an incredibly low value. Material absorption and Rayleigh scattering contribute dominantly to the fiber loss spectrum. Pure silica absorbs either in ultraviolet region or in the far infrared region beyond 2 μm. However, even a relatively small amount of impurities can lead to significant absorption in the wavelength window 0.5 – 2 μm. The most important impurity that affects the fiber loss is the OH ion, which has a fundamental vibration absorption peak at about 2.73 μm. The overtones of the OH absorption peak are responsible for dominant

peak near 1.37 μm and a smaller peak near 1.23 μm. Narrow windows exist in the longer wavelength region around 1.3 μm and 1.55 μm which are essentially unaffected by OH absorption once impurity level has been reduced below one part in hundred million. This situation is illustrated in Fig. 1.12.

Rayleigh scattering is a fundamental loss mechanism arising from random density fluctuations frozen into fused silica during manufacture. Resulting local fluctuations in the refractive index scatter light in all direction. The Rayleigh scattering loss varies as λ^{-4} and is dominant in short wavelengths. Since this loss is intrinsic to the fiber, it sets the ultimate limit on the fiber loss. The intrinsic loss is estimated to be

$$\alpha_R = \frac{C}{\lambda^4} \tag{1.3}$$

Where the constant C is in the range of $0.7 - 0.9$ dB/(km-μm^4) depending on the constituents of the fiber core. Since $\alpha_R = 0.12$-0.15 dB/km at $\lambda = 1.55$ μm, the fiber loss is dominated by Rayleigh scattering. Other factors that may contribute to the fiber loss are bending losses and boundary losses (due to scattering at the core-cladding boundary). The total loss of a fiber link in optical communication systems also includes the splice losses to a level of ~0.01 dB.
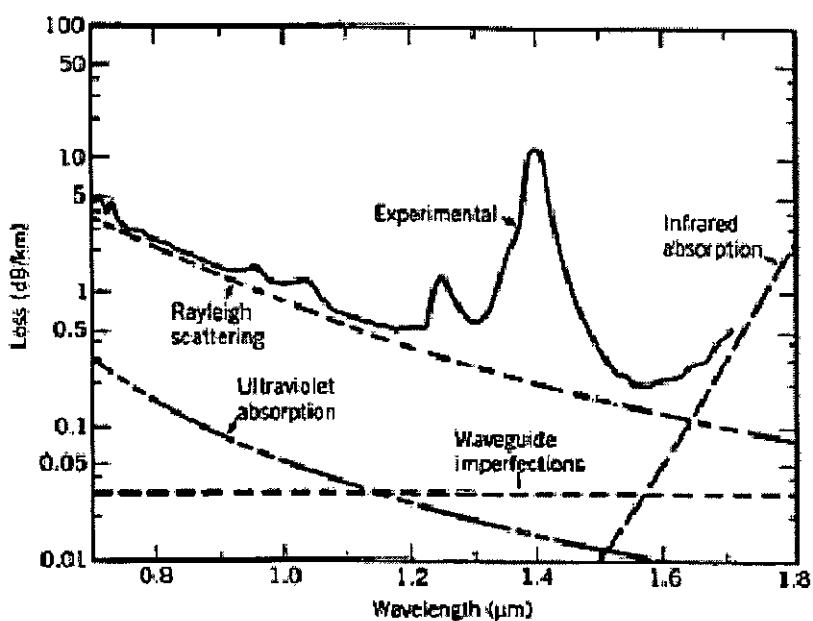
Fig. 1.11: The measured attenuation spectrum for an ultra-low-loss single mode fiber (solid line) with calculated attenuation spectra for some of the loss mechanisms contributing to the total fiber attenuation (dashed and dotted lines). [Miya, 1979]
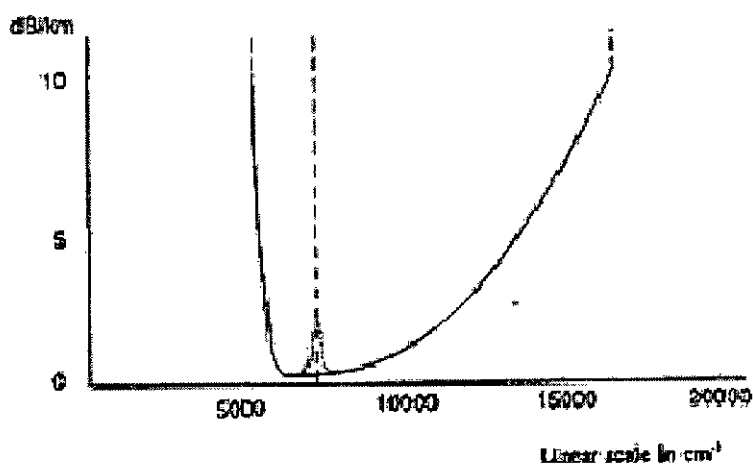
Fig. 1.12: Typical loss of a low OH contents fiber. The low-loss window is from about 5,300 to 16,000 cm^{-1} in wave number ($\sigma=1/\lambda$).

1.4.2 Dispersion

Dispersion of transmitted optical signal causes distortion for both digital and analog transmission along optical fibers. The velocity of transmission of electromagnetic wave through transparent materials is influenced by the interaction of the waves with the atoms of the material. As the interaction is a function of wave frequency, the velocity of the wave propagation is dependant on the wave frequency. Consequently, short pulses of light tend to be spread out as they propagate. The spread is proportion to the range of optical frequencies in the pulse and constitutes an important factor in limiting the bandwidth of optical fiber. This phenomenon is known as dispersion [Gower, 1993]. While each pulse broadens, it overlaps with its neighbors as shown in Fig.1.13, eventually becomes indistinguishable at the receiver input. The effect is known as inter symbol interference (ISI). Thus an increasing number of errors are encountered on the digital optical channel as the ISI become more pronounced.

The dispersion is of two types, namely, intramodal dispersion and intermodal delay effect. Intermodal delay occurs in multimode transmission and is a result of each mode having a different group velocity at a single frequency. Intramodal dispersion is commonly referred to as chromatic dispersion. Intramodal dispersion is the pulse spreading that occurs within a single mode transmission and is a result of the phase velocity being a function of the wavelength. The causes of intramodal dispersion are:

- Material dispersion that arises from the variation of the refractive index of the core material as a function of the wavelength. It is the principle factor in determining the dispersion effect.
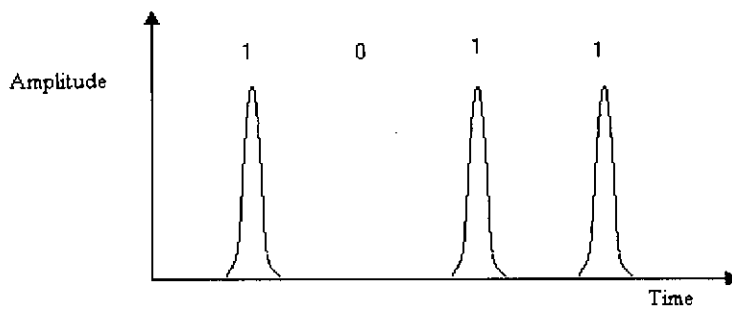
(a)
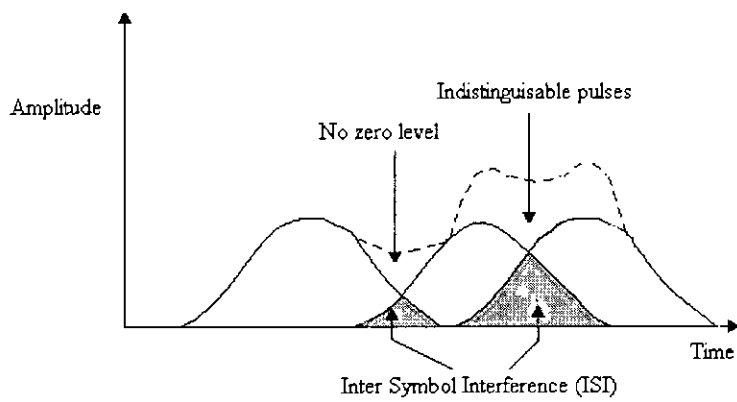
(b)

Fig. 1.13: An illustration using the digital bit pattern 1011 of the broadening of light pulses as they are transmitted along a fiber: (a) fiber input; (b) fiber output at a distance L.

- Waveguide dispersion, which occurs because the modal propagation constant is a function of optical fiber dimension relative to the wavelength.

1.4.3 Nonlinear Effects

With the evolution of low loss single mode fibers, nonlinear effects become more dominant now a day than the multimode fiber regime, because certain nonlinear phenomenon depends on optical power level density with the long haul transmission. It is possible to gain that level with only a few milliwatts of power of single mode fiber. Again when optical channels are multiplexed and the launched power in each channel is increased, nonlinear effects put limitations on the system. There exists a rich collection of nonlinear optical effects in fused silica fibers, each of which manifests itself in a unique way [Chraplyvy, 1990]. Stimulated Brillouin scattering (SBS), the interaction between light and sound waves in the fiber, causes frequency conversion and reversal of the propagation direction of light. Cross phase modulation (XPM) is an interaction, via nonlinear refractive index, between the intensity of one light and the optical phase of other light waves. Four-photon mixing (FWM) is analogous to third order intermodulation distortion whereby two or more optical waves at different wavelength mix to produce new optical waves at other wavelength. Stimulated Raman scattering (SRS), an interaction between light and vibration of silica molecules, causes frequency conversion of light and results in excess attenuation of short-wavelength channels in wavelength-multiplexed systems.

Each of these nonlinearities will affect specific lightwave systems in different ways. However in general, SRS, SBS and FWM will deplete certain optical waves and by means of frequency conversion, will generate interfering signals for other channels. These will

degrade both direct detection (DD) and heterodyne systems. XPM, on the other hand, affects only the phase of other signals. Consequently, only angle-modulated systems will be affected by this nonlinearity.

Most nonlinear optical interactions involving two overlapping optical waves propagating in a medium can be characterized generally by,

$$P_1(L) = P_1(0) \exp(gP_2 L / A) \qquad (1.4)$$

Where $P_1(0)$ and $P_1(L)$ is the power of one wave entering and exiting, respectively in the medium of length L. This amplified wave is commonly called the probe wave. P_2 is the injected power of the other wave, called the pump, which generates the gain for the first wave. The cross-sectional area common to the light beams is A; the gain coefficient g (expressed in cm/W) is a direct measure of the strength of nonlinearity. Equation 1.4 assumes that P_2 is constant throughout the nonlinear medium that is no pump depletion due to nonlinearity and no intrinsic loss. Furthermore, (1) assumes that the polarization states of the pump and probe waves are the same. Neither of these assumptions typically hold good in fibers. Attenuation in long fibers is not negligible and the polarization states of the pump and probe waves can evolve differently in the fiber. Consequently, (1) must be modified to be applicable to single mode fibers [Smith, 1972]. The correct expression is,

$$P_1(L) = P_1(0) \exp(gL_{eff} P_2 L / bA_{eff}) \qquad (1.5)$$

where $P_1(0)$ $P_1(L)$ and g are defined as before. The effective area of the propagating waves A_{eff} is evaluated by calculating the average modal overlap between the pump and probe waves [Hill, 1978], [Stolen, 1979, 1982]. However, in general, if the pump and probe

wavelengths are comparable and both are slightly longer than the fiber cutoff wavelength, then $A_{eff} = A$, where A is the core area of the fiber [Johnson, 1977]. The effective fiber length L_{eff} replaces the actual length L in order to account for the exponential decay of the pump power with length due to fiber loss (Fig. 1.6). A simple integration shows that

$$L_{eff} = \frac{1 - e^{-\alpha L}}{\alpha} \qquad (1.6)$$

where α is the loss coefficient of the fiber. For $\alpha L << 1$, $L \approx L_{eff}$, and for $\alpha L >> 1$, $L \approx 1/\alpha$. Factor b accounts for polarization of pump and probe waves and the polarization properties of the fiber. In a polarization-maintaining fiber, with identical pump and probe polarization states, $b = 1$. In a conventional fiber that does not maintain polarization states, $b = 2$.
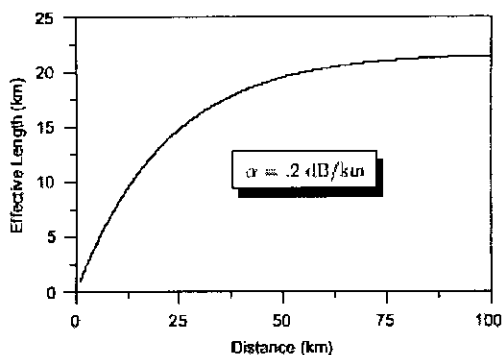
Fig. 1.14: Relation between Effective length and fiber length considering attenuation coefficient $\alpha=0.2$ dB/km.

1.5 Background of this Study

During the last thirty years or so the study of nonlinear effects in the optical fibers has led to the advent of a new branch of nonlinear optics, referred to as nonlinear fiber optics. A large number of research projects and developments have been carried out over the years in this field. Stimulated Raman and Brillouin scatterings in single-mode optical fibers were studied as early as in 1972 both experimentally [Stolen, 1972], [Ippen, 1972] and theoretically [Smith, 1972]. These works stimulated the other nonlinear phenomena such as optically induced birefringence [Stolen, 1973(b)], parametric four-wave mixing [Stolen, 1974, 1975] and self-phase modulation [Ippen, 1974], [Stolen, 1978]. An important contribution was made in 1973 when it was suggested that optical fibers can support soliton-like pulses as a result of an interplay between the dispersive and nonlinear effects [Hasegawa, 1973]. Optical solitons have later been observed [Mollenauer, 1980] and have led to a number of advantages in the generation and control of ultrashort optical pulses [Mollenauer, 1984, 1986], [Kafka, 1987], [Islam, 1987] and [Gouveia-Neto, 1988]. Their use in optical communication systems is also likely to lead to new performance achievements. An equally important development is related to the use of optical fibers for pulse compression [Nakatsuka, 1981], [Shanak, 1982], [Nikolaus, 1983(a), 1983(b)] and [Gomes, 1988]. Pulses as short as 6 femtosecond (fs) (1 fs = 10^{-15}) have been generated using fiber based nonlinear compression techniques [Fork, 1987].

New developments are being made almost regularly in the field of nonlinear fiber optics. Phenomenon such as cross-phase modulation and soliton switching attracted considerable attention during 1980s [Boyd, 1992]. A new dimension was added when optical fibers

were doped with rare-earth elements and used to make amplifiers and lasers [Poole, 1986]. Research on erbium-doped fiber amplifiers and lasers intensified during 1990s to the extent that such devices became available commercially by 1992 [Agrawal, 1995].

Today's communication system requires large transmission capacity for multimedia communication, which can only be met up using WDM technique [Norimatshu, 2001]. However, performance of a high power WDM system is ultimately degraded due to Raman induced crosstalk effects [Tariq, 1993].

The SRS causes power transfer from shorter-wavelength WDM channels to longer-wavelength WDM channels and thus induces interchannel modulation between each WDM channel [Ho, 2000]. The optical power limits are calculated by the worst-case assumption that all WDM channels are synchronized and transmitted at ONE level simultaneously [Chraplyvy, 1983]. The influence of fiber dispersion is also included in the analyses [Cotter, 1984], [Wang, 1998].

In all these calculations of Raman crosstalk, the experimentally found Raman gain profile of silica reported in [Stolen, 1980] is approximated by a triangular function (referred to Fig. 2.5), where the peak Raman gain occurs at 15 THz spacing between channels and no Raman gain is assumed at larger spacing [Chraplyvy, 1984]. The results so far reported in literature based on this approximation are sufficiently accurate as long as the bandwidth of the fiber amplifier available currently is concerned [Norimatshu, 2001]. However, for future wideband WDM system, this approximate model of Raman gain will produce inaccurate results and therefore, it requires developing an improved model for the Raman gain.

The probability density function (PDF) of SRS induced crosstalk is developed [Ho, 2000], [Forghieri, 1995]. However, the complete performance evaluation based on the statistical analysis of Raman crosstalk is yet to be reported. The overall system limitations due to the SRS effect are not quantified in the literature to help in designing an optical WDM system for future communication.

1.6 Objective of this Study

The objective of this work is to develop an improved model to fit the experimentally found Raman gain profile. This model will then be utilized to calculate accurately the power depletion of the shortest-wavelength channel due to the SRS effects from all possible channels in a wide-band WDM system. Based on this improved model, the performance analysis techniques of a WDM system will be modified and generalized. From the evaluated performance of the WDM system, the limitations on the launched power will be estimated.

This work will also include a complete statistical analysis of the WDM system. The probability density function (pdf) of the power depletion of the shortest channel will be evaluated. Then the bit error rate (BER) performance of the WDM system will be determined. From the BER characteristics, the power penalty suffered by the system will be evaluated for various combinations of system parameters. Finally, the system limitations for a given maximum penalty will be quantified.

1.7 Organization of the Thesis

The thesis consists of five chapters. Chapter 1 introduces the background of this topic and objective of this work with a brief discussion of previous works in this field.

Chapter 2 deals with basics of SRS and its effect on the performance degradation of WDM systems. Experimentally found Raman gain spectrum of silica and its triangular approximation used in various literatures are also introduced.

In Chapter 3 an improved model for the Raman gain profile is proposed which in turn is used to estimate the power depletion of the shortest wavelength channel due to all other channels in the system. The power penalty suffered by the system due to SRS crosstalk as well as the system limitations are estimated.

Chapter 4 includes the performance evaluation based on the statistical analysis of Raman crosstalk, which is developed to estimate the system bit error rate (BER).

Finally, chapter 5 lists the results of this work and their technical contributions to the field of WDM system. It also suggests several research projects in continuation and further development of the present work.

Chapter 2

STIMULATED RAMAN SCATTERING

2.1 Introduction

Stimulated Raman scattering (SRS) describes the parametric interaction of light with molecular vibrations [Boyd, 1992]. It is an important nonlinear process that can turn optical fibers into broadband Raman amplifiers and tunable Raman lasers [Chraplyvy, 1990]. It can also limit the performance of multichannel optical communication systems by transferring the energy from one channel to the neighboring channels [Chraplyvy, 1990, 1993]. Raman induced crosstalk in a multichannel optical communication system is the ultimate power limiting phenomenon which causes performance degradation [Tariq, 1993], [Chraplyvy, 1993], [Wang, 1998].

This chapter describes the basic concepts of SRS and its effect on the performance of wavelength division multiplexed (WDM) system. Performance evaluation of WDM system based on the triangular approximation of Raman gain spectrum is described which includes analytical expression of power depletion.

2.2 Scattering Phenomena

When an optical wave is within a fiber medium, incident photons may be scattered,

producing a phonon emitted at acoustic or optical frequencies by exciting molecular

vibrations, together with another photon at a shifted frequency. This process can be stated as

the molecule absorbing the photon at original frequency and simultaneously making

transition between vibrational states. The scattered photon therefore emerges at a frequency

shifted below or above the incident photon frequency with the energy difference between the

incident and scattered photon. The up shifted scattered wave is known the as Stokes

component whereas the downshifted one is known as the anti-Stokes component. In contrast

to linear scattering (i.e., Rayleigh), which is known as elastic, as the scattered waves

preserve the frequency of incident wave, these nonlinear scattering processes are clearly

inelastic. The small inelastic scattering frequency shifts, which are caused for acoustic

phonon generation typify Brillouin scattering whereas large shifts are caused for optical

phonon, indicating Raman scattering.
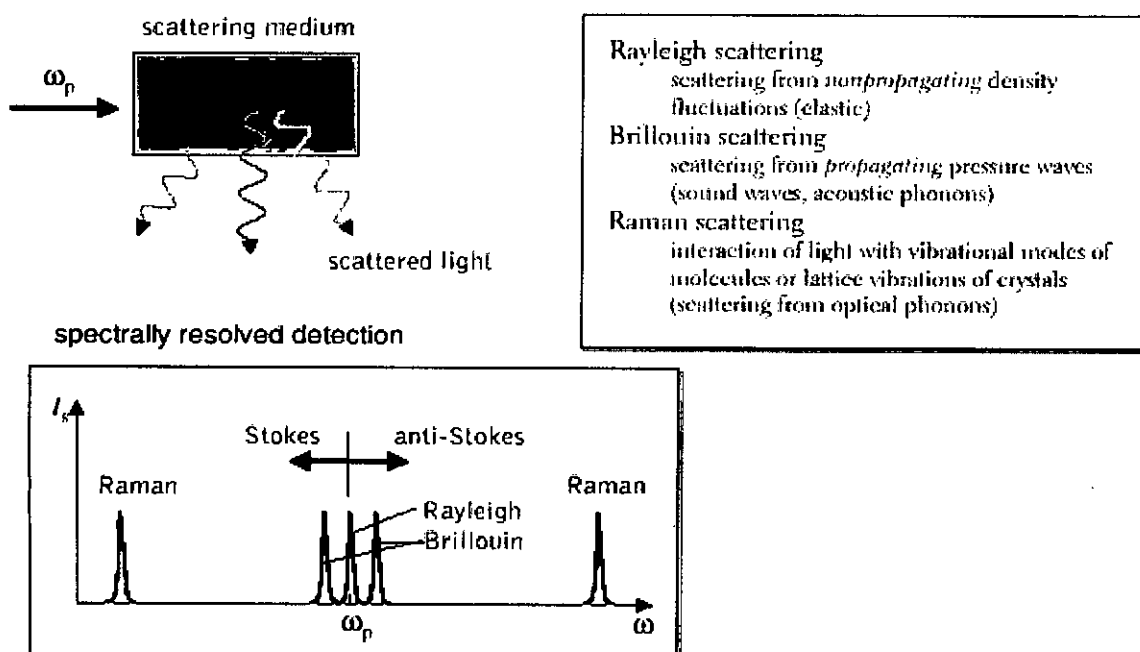
Fig. 2.1: Comparison among different types of scattering.

2.2.1 Spontaneous Raman Scattering

The spontaneous Raman effect was discovered by C. V. Raman in 1928. In spontaneous Raman effect, a beam of light illuminates a material sample (which can be a solid, liquid or gas) and is scattered. In general, the scattered light contains frequencies different from those of the excitation source. Those new components shifted to lower frequencies are called Stokes lines and those shifted to higher frequencies are called anti-Stokes lines. The Stokes lines are more intense than the anti-Stokes lines in order of magnitude.

These properties of Raman scattering can be understood through use of the energy level diagram as shown in Fig. 2.2. Raman Stokes scattering consists of a transition from the ground state to a virtual level associated with the excited state followed by a transition from the virtual level to the final state. Raman anti-Stokes scattering entails a transition from final state to ground state with the virtual state serving as the intermediate level. The anti-Stokes lines are typically much weaker than the Stokes lines because, in thermal equilibrium, the population of final state is smaller than the population in ground state by the Boltzman factor $exp\ (\hbar\omega_{ng}\ /\ kT)$.

2.2.2 Stimulated Raman Scattering

SRS occurs when sufficiently large pump wave is co-injected at a lower wavelength than the signal to be amplified. In spontaneous Raman scattering, incident light is scattered at a down shifted (stokes-shifted) frequency. This process is strongly dependent on the power of the incident beam, called the pump. As the pump power increases, the scattering

increases until the scattered power reaches a threshold level. If the pump power is increased beyond this limit, scattering becomes stimulated and the pump rapidly losses its power to Stokes-shifted beam. The pump then is said to be depleted due to SRS.

The threshold power level in the bulk material is usually large. SRS in the bulk material is usually obtained using high power Q-switched lasers. The material, which produces the Stokes shifted beam, is often placed inside a cavity to increase the gain due to feedback.

In the optical fiber, however SRS can be observed at relatively low pump power levels without any feedback. This is possible because the core size of the fiber is very small, producing large power density at relatively low total power. Moreover, the intensity can be kept almost constant for long distances because of the waveguide nature of the fiber and its low attenuation coefficient.

SRS process is proportional to the product of the number of pump and Stokes photons present at the same point in the fiber. Since spontaneous Raman scattering is not a first order process, the pump power must be large enough to produce the minimum number of scattered photons, which can initiate the SRS process.

SRS rises from a third order nonlinear susceptibility, which has subpicosecond time constant. Since this is essentially instantaneous compared to modulation rates in lightwave systems, SRS effects will be the same for both modulated and continuous wave.

✓ Typically $\omega_m \sim 10^2 - 10^3$ 1/cm

✓ Weak interaction process ($\sigma_{\_\_\_\_\_} \sim 10^{\_\_}$ cm²)

✓ Emission isotropic

✓ Used to map out vibrational and rotational structure of molecules in gas, liquid or solid phase

✓ Two-photon process: Allows study of molecular vibrations which are not infrared-active

      Levels E_a and E_a have same parity
      ⇒ direct electric dipole transition forbidden

Rotational Raman spectrum
of C_2N_2 excited with 488 nm
laser light
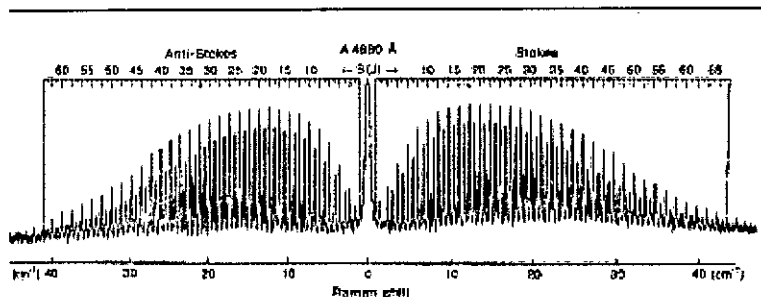
(a)

For strong pump fields the number of emitted Raman photons is high
⇒ they can stimulate further (coherent) Raman photons to be emitted
   in the direction of the pump beam
⇒ gain !

generation of stimulated
Stokes radiation

$$\hbar\omega_p + \hbar\omega_s = 2\hbar\omega_s + \hbar\omega_m$$

Stokes - anti-Stokes
coupling
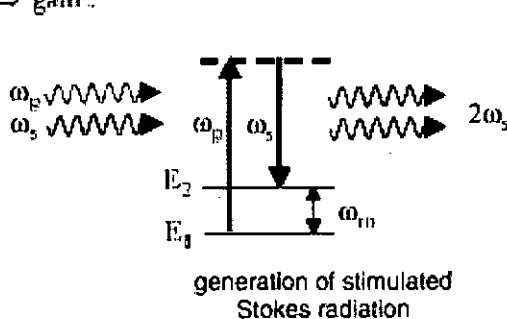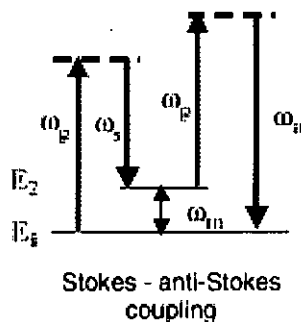
⇒ Stokes and anti-Stokes waves
can have comparable intensities

(b)

Fig 2.2: A brief overview on Raman Scattering, (a) Spontaneous Raman Scattering with a typical spectrum found from experimental result, (b) Stimulated Raman Scattering with a schematic view.

2.3 Effect of SRS on WDM System Performance

In WDM systems, stimulated Raman signals do not build up from weak spontaneous Raman noise. They are generated from relatively strong signals carried by the fiber and therefore the effect of SRS can be enhanced by many orders. In a single-channel lightwave system only one wavelength of light is injected into the fiber. However this signal generates spontaneous Raman scattered light, which can be amplified. It has been shown both theoretically [Smith, 1972], [Stolen, 1980] and experimentally [Stolen, 1984] that amplification of light will cause severe degradation (50% signal degradation) when $gL_{eff}P/bA_{eff}$ of (1.5) equals to 16. For the assumed system parameters (Appendix A), the injected signal power required to produce system degradation is about 1 W. It is clear that effect of SRS will not be significant for single channel silica fiber based lightwave systems.

The effect of SRS in a two-wavelength system is an increase in light intensity at one wavelength at the expense of light intensity at a slightly shorter wavelength [Chraplyvy, 1983]. This exchange of power between different wavelength channels has been called 'stimulated Raman crosstalk'.

Let us assume that a two-channel amplitude modulated WDM system has channel spacing such that SRS couples the two channels. This assumption is usually satisfied, because the broad stimulated Raman gain profile of silica ensures that there will be some channel coupling in most cases. Let channel 1 operate at wavelength λ_1, which is shorter than λ_2, the wavelength of channel 2. Let us call channel 1 the pump channel and channel 2 the probe channel. If initially two channels have equal optical power injected into the fiber

then the probe channel (λ_2) is intensified and the pump channel (λ_1) is depleted. In a segment of fiber of length ΔL, and assuming scrambled polarization, the amplified probe power is given by

$$P_2(L + \Delta L) = P_2(L)\exp\left(\frac{\gamma P_1(L)\Delta L}{2A_{eff}}\right) \qquad (2.1)$$

where, γ is the SRS gain coefficient and A_{eff} is the effective core area of the fiber. The pump is depleted by

$$P_1(L + \Delta L) = P_1(L) - \frac{\lambda_1}{\lambda_2}[P_2(L + \Delta L) - P_2(L)] \qquad (2.2)$$

For a 50 km fiber with an effective core diameter of 8 μm and a stimulated Raman gain coefficient $\gamma = 7 \times 10^{-12}$ cm/W (this corresponds to a channel spacing of 100 nm at 1.5 μm), the received pump and probe powers as a function of injected powers for a fiber with $\alpha = 0.25$ dB/km are shown in Fig. 2.3. It represents that received power does not increase monotonically with input power. Increasing the transmitter power above 50 mW actually results in lower received power in the pump channel. Therefore, there is a maximum usable transmitter power that can be injected into a short-wavelength channel. This maximum power scales directly with fiber loss and is significantly smaller than the SBS thresholds [Cotter, 1982].

The pump and probe power can be calculated for equal group velocities of two channels. The effects of two different group velocities do not change the results because the system degradation is determined by worst-case interaction, which consists of a

mark in one channel interacting with a series of marks in the other channel. With angle modulation the digital message to be conveyed is impressed on the phase angle of the optical carrier, rather than on the amplitude, which is normally constant. In this case the gain in the probe channel is uniform rather than sporadic, because the optical intensities are unmodulated. In multichannel systems, the shortest wavelength channel experiences the worst degradation and the longest wavelength channel experiences either no degradation for amplitude shift keying (ASK) or perhaps an improvement in signal to noise ratio (angle modulation). All the intermediate channels will experience some degradation, the magnitude of which depends on their location in the sequence of wavelengths.

Analytical expression was derived to estimate transmitter power limitations due to SRS for multichannel WDM system [Chraplyvy, 1984]. These results are applicable to systems containing an arbitrary number of channels with arbitrary (but equal) channel separation. A WDM system having N equally spaced channels with channel separation Δv (Hz) is assumed. The degradation caused by SRS was found to be the most severe for the shortest wavelength channel (called zeroth channel). Therefore, system performance limits can be estimated by calculating the depletion of the zeroth channel. Maximum depletion occurs when there is a binary ONE (optical power 'on') in each channel [Chraplyvy, 1984]. In this case assuming scrambled polarization and the Raman gain to be in the linear regime, the fractional power D lost by the shortest-wavelength channel (which is also called depletion) is given by [Chraplyvy, 1984]

$$D = \sum_{i=1}^{N-1} \frac{\lambda_i}{\lambda_0} \frac{P_i \gamma_i L_e}{2A} \qquad (2.3)$$

where, P_i is the injected power (watts) in the ith channel, λ_i is the wavelength of ith channel, γ_i is the Raman gain coefficient coupling the ith and the shortest wavelength channel, A is the effective core area given by the appropriate overlap integrals [Mittra, 1971], and L_{eff} is the effective fiber length as stated in (1.6).

Equation 2.3 was derived [Chraplyvy, 1984] assuming no Raman interaction among the other N-1 channels, i.e. the various P_i are assumed to remain constant over the length L_e. In case of linear Raman gain the error arising from this assumption is less than 1%. To facilitate calculation it is assumed that the λ_i and P_i are the same for all channels.

The power penalty X (dB) is the amount of power that has to be compensated for overcoming degradation due to SRS and is given by [Chraplyvy, 1984]

$$X = -10\log(1-D) \qquad (2.4)$$

In a system of N channels with channel spacing Δv and the power P per channel, no channel will experience a 1 dB penalty provided $[NP][(N-1)\Delta v] < 500$ GHz .W. It is to be noted that NP is the total optical power and $(N$-1$)\Delta v$ total occupied optical bandwidth. Therefore, the product of total optical power and total optical bandwidth must be smaller than 500 GHz .W to reduce the degradation due to SRS to an acceptable level.

2.4 Raman Gain Profile

Raman gain coefficient is related to the imaginary part of third order nonlinear susceptibility [Shen, 1984], [Boyd, 1992]. It can be calculated using a quantum-mechanical approach. For silica fibers it was measured by Stolen *et al.* [Stolen, 1972, 1973]. The pump power level, where the SRS becomes important, is defined as critical power, P_{crit}. A detailed analysis by Smith [Smith, 1972] shows that this power level is given by,

$$P_{crit} = 16 A_{eff} \frac{\alpha_p}{\gamma_p} \tag{2.5}$$

where A_{eff} = effective core area, γ_p = peak Raman gain coefficient, and α_p = fiber attenuation coefficient for the pump.

Figure 2.4 shows the Raman gain coefficient (γ) for fused silica as a function of the frequency shift at a pump wavelength λ_p = 1 μm [Stolen, 1980]. For other pump wavelengths, γ_p scales inversely with λ_p. The most significant feature of the Raman gain in silica fibers is that γ extends continuously over a large frequency range (up to 40 THz) with a broad peak near 15 THz at a pump wavelength λ_p=1.55 μm. This behavior is due to the non-crystalline nature of silica glass. It is almost linear up to about 15 THz, where it reaches its peak value. Beyond 15 THz, the gain reduces gradually and becomes negligible at higher frequency shifts.
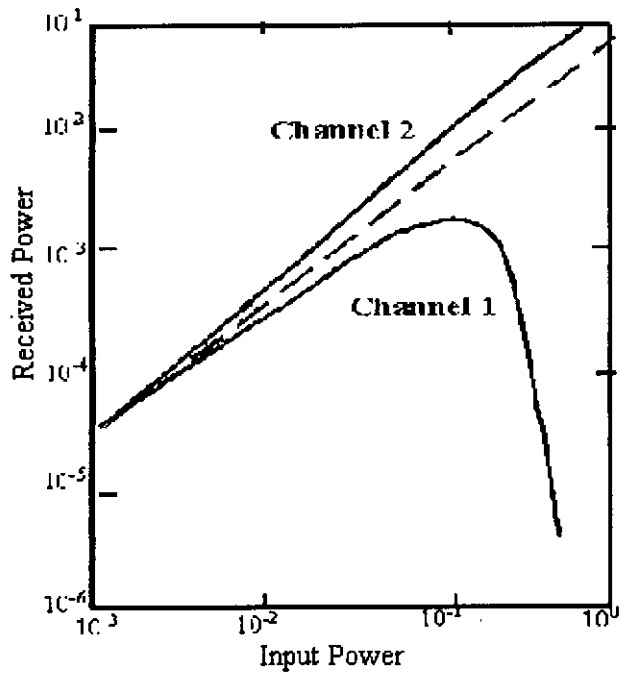
Fig. 2.3: Received power against input power of channel 1 (pump) and channel 2(probe) in the presence of stimulated Raman interaction in a 50 km fiber with 0.25 dB/km loss.
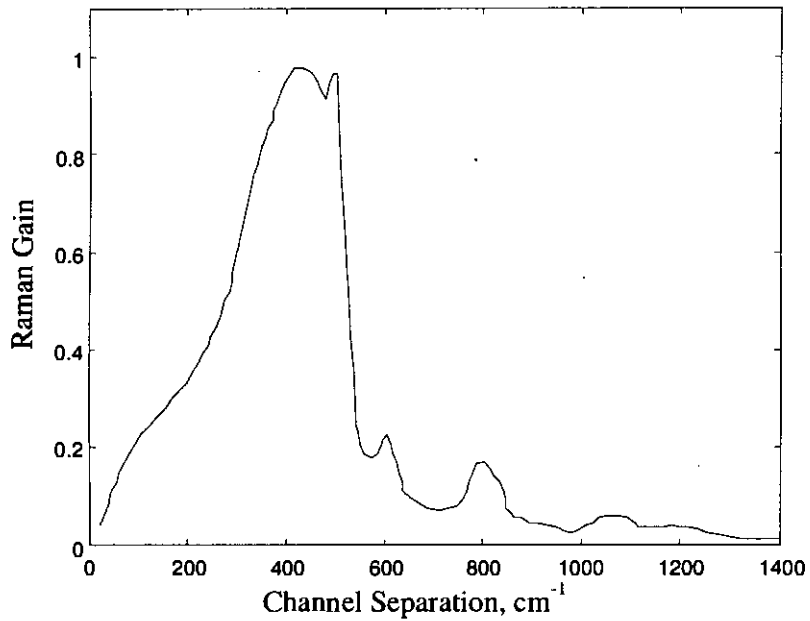
Fig. 2.4: Experimental Raman gain spectrum.

2.5 Performance Evaluation of WDM System Based on Previous Estimation

In the performance evaluation of WDM systems [Chraplyvy, 1984], actual Raman gain profile of silica is approximated by a triangular function [Chraplyvy, 1984], [Forghieri, 1995], [Christodoulides, 1996] and [Ho, 2000] where the Raman gain increases linearly with channel spacing and the peak gain coefficient, γ_p, occurs at 500 cm^{-1}, while there is no Raman interaction beyond this point as shown in Fig. 2.5.

Due to this triangular approximation, there are two possibilities to consider. Firstly, all the channels fall within the Raman gain profile, i.e. $(N\text{-}1)\,\Delta v < 1.5 \times 10^{13}$ Hz, and in this case the depletion of the shortest-wavelength channel is given by

$$D_1 = \frac{\Delta v \gamma_p P L_e}{3 \times 10^{13} A} \frac{N(N-1)}{2} \tag{2.6}$$

For typical system parameters, i.e. $\alpha = 0.25$ dB/km, $A = 5 \times 10^{-7}$ cm^2, $\gamma_p \sim 6 \times 10^{-12}$ cm/W, and equation (2.6) thus reduces to

$$D_1 = 3.3 \times 10^{13} P \Delta v N(N-1) \tag{2.7}$$

Secondly, for the assumption of $(N\text{-}1)\,\Delta v > 1.5 \times 10^{13}$ Hz, only $M = 1.5 \times 10^{13}/\Delta v$ channels will contribute to depletion of the zeroth channel. In this case if $M >> 1$ then D is given by

$$D_1 = 7.4 \times 10^{13} \frac{P}{\Delta v} \tag{2.8}$$

and is independent of the total number of channels.

If a penalty $X < 0.5$ is required then the maximum allowable transmitter power per channel for the two cases can be determined as

$$P_1 < \frac{3.3 \times 10^{11}}{\Delta \nu N(N-1)} \qquad (2.9)$$

and

$$P_1 < 1.5 \times 10^{-15} \Delta \nu \qquad (2.10)$$

These inequalities can now be used to estimate the transmitter power limits for a wide variety of WDM systems. When all the channels fall within the Raman gain profile, the maximum allowable total optical power injected into the fiber (P_1N) scales inversely with the total occupied bandwidth $(N\Delta\nu)$.
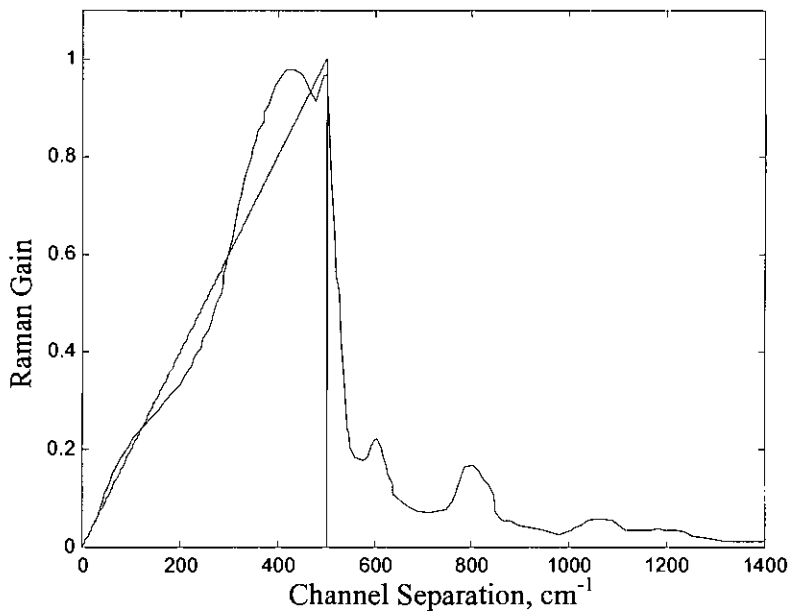
Fig. 2.5: Triangular approximation of Raman gain profile [Chraplyvy, 1984].

2.6 Results and Discussion on the Performance Analysis Based on Triangular Assumption

Figure 2.6 shows the estimated power depletion as a function of the number of channels considering triangular approximation of Raman gain profile [Chraplyvy, 1984]. It is obvious that there is sharp rise in depletion with the increase in number of channels within the linear regime of Raman gain profile, the value of depletion then saturates. This is because after the linear regime Raman gain is assumed to be zero. So if a channel falls in the remaining regime it has no effect on depletion.

Fig. 2.7 shows the power penalty suffered by the shortest channel due to the SRS effect arising from all the channels in the system considering triangular approximation of Raman gain profile [chraplyvy, 1984]. As the number of channels increases, the depletion increases causing more power penalty for a WDM system. It can be seen that the power penalty increases within the linear regime of Raman gain profile, the value of power penalty then saturates. This is because after the linear regime Raman gain is assumed to be zero. Therefore, if a channel falls in the remaining regime it has no effect on the power penalty. The penalty also increases with the power input to the system.

Figure 2.8 shows the power penalty for different effective lengths of the fiber. Note that the power penalty increases within the linear regime of Raman gain profile, the value of power penalty then saturates. This is because after the linear regime Raman gain is assumed to be zero. The power penalty also increases as the fiber effective length

Fig. 2.6: Depletion profile as a function of number of channels for typical system parameters, $\alpha = 0.25$ dB/km, $A_{eff} = 5 \times 10^{-7}$ cm^2, $\gamma_p \sim 6 \times 10^{-12}$ cm/ W^2, launched power= 1 mW, channel separation, $\Delta\lambda \sim 10$ nm ($\Delta v \sim 1.3 \times 10^{12}$ Hz at 1.5 µm).
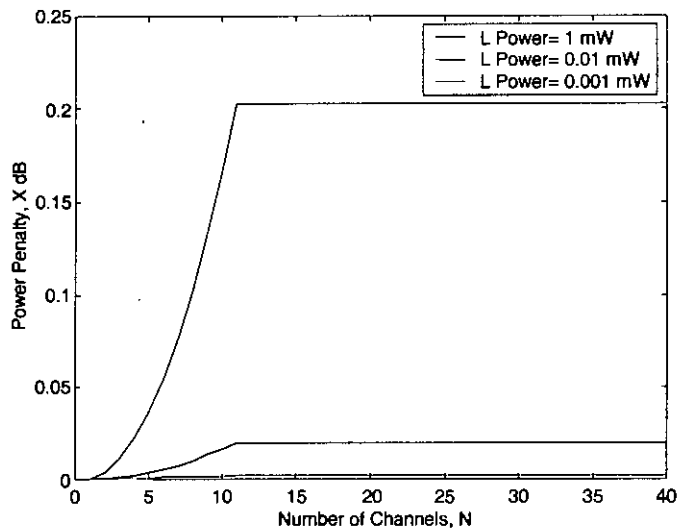
Fig. 2.7: Power penalty for different input power as a function of number of channels using typical system parameters, effective length = 16 km, effective core area, $A_{eff} = 5 \times 10^{-7}$ cm^2, $\gamma_p \sim 6 \times 10^{-12}$ cm/ W^2, launched Power = 1 mW, channel separation, $\Delta\lambda \sim 10$ nm ($\Delta v \sim 1.3 \times 10^{12}$ Hz at 1.5 µm).
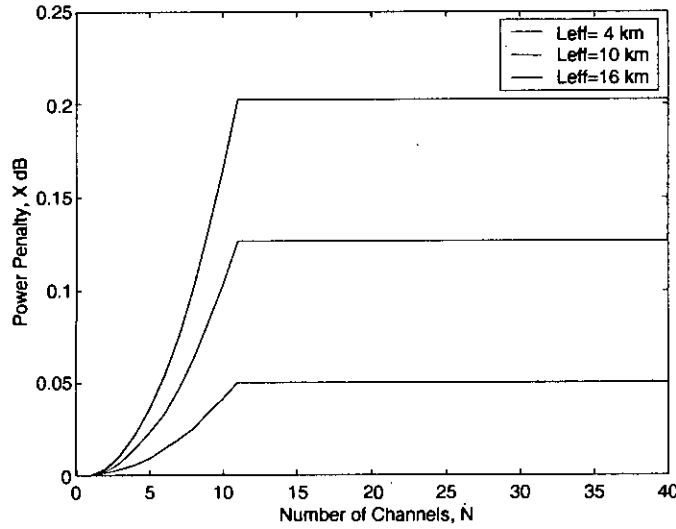
Fig. 2.8: Power penalty for different effective length as a function of number of channels using typical system parameters, $\alpha = 0.25$ dB/km, $A_{eff} = 5 \times 10^{-7}$ cm^2, $\gamma_p \sim 6 \times 10^{-12}$ cm/ W^2, launched Power = 1 mW, channel separation, $\Delta\lambda \sim 10$ nm ($\Delta v \sim 1.3 \times 10^{12}$ Hz at 1.5 μm).

increases. All these are because of the increasing amount of crosstalk due to the SRS effect.

2.7 Conclusion

The basic concepts of SRS and its effect on WDM systems are discussed. The SRS causes performance degradation by transferring energy from shorter wavelength channel to the larger wavelength channel. The performance evaluation of multichannel system using triangular approximation of Raman gain profile is stated. Analytical expressions for calculating power depletion and power penalty is presented. These expressions can be used to estimate the transmitter power limits for a wide variety of WDM systems.

Chapter 3

PERFORMANCE EVALUATION OF WIDE BAND WDM SYSTEM

3.1 Introduction

In the performance evaluation of a wavelength division multiplexed (WDM) system under the effect of stimulated Raman scattering (SRS), experimentally found Raman gain profile of silica reported in [Stolen, 1980] is approximated by a triangular function. The results reported so far in literature based on this approximation are sufficiently accurate as long as the bandwidth of fiber amplifiers available at this moment is concerned [Norimatsu, 2001]. However, for future wide band WDM systems, this approximate model of Raman gain will fail, and therefore, it requires developing an improved model for the Raman gain.

In this chapter, an improved model is developed to fit the experimentally found Raman gain profile. This model is then utilized to calculate more accurately the power depletion of the shortest-wavelength channel due to the SRS effects from all possible channels in a wide-band WDM system. Based on this improved model, the performance analysis of a WDM system is modified and generalized. From the performance results of the WDM system, the limitations on the launched power will be estimated.

3.2 Improved Raman Gain Profile

Figure 3.1 shows that in the actual Raman gain profile of silica Raman gain coefficient is still significant beyond 15 THz spacing between channels for a pump wavelength of 1.55 μm. This tail of the Raman gain spectrum is not accounted for in the triangular approximation. Therefore, the second possibility considered in [Chraplyvy, 1984] contributes significant amount of error. With the proposed model, the SRS effects from channels at the tail of Raman gain profile are taken into account. The actual Raman gain profile is divided into three regions of channel spacing.

In Region I (channel spacing up to 15 THz), the Raman gain profile of silica is assumed to be a linearly increasing function from zero to peak Raman gain coefficient γ_p, which is inversely dependant on the pump wavelength,

$$\gamma_i = \frac{(i\Delta v)\gamma_p}{1.5 \times 10^{13}} \quad , \qquad i\Delta v < 1.5 \times 10^{13} \, \text{Hz} \tag{3.1}$$

In Region II (channel spacing from 15 THz up to 16.5 THz), the gain profile is assumed to be a linearly decreasing function,

$$\gamma_i = \{(-6.087 \times 10^{-13} \times i\Delta v) + 10.06382\}\gamma_p, \tag{3.2}$$

for $1.5 \times 10^{13} \, Hz \leq i\Delta v \leq 1.65 \times 10^{13} \, \text{Hz}$

In Region III (channel spacing beyond 16.5 THz), the profile is assumed to be an exponentially decreasing function,

$$\gamma_i = a\gamma_p \exp\left\{\frac{-(i\Delta v - x_0)}{b}\right\} \qquad (3.3)$$

where $a = 0.24168$, $x_0 = 1.62 \times 10^{13}$, $b = 8.64655 \times 10^{12}$.

3.3 Power Depletion

In [Chraplyvy, 1984] using triangular approximation, depletion has been calculated for two possibilities. First, it is assumed that all the channels fall within the Raman gain profile, i.e. $(N-1) \Delta v < 1.5 \times 10^{13}$ Hz. Second, it is assumed that $(N-1) \Delta v > 1.5 \times 10^{13}$ Hz; only $M = 1.5 \times 10^{13}/\Delta v$ channels contribute to depletion of shortest wavelength channel. Result for the first case is accurate. For the second case, since no Raman gain coefficient is considered at larger spacing, some error is introduced in calculating the depletion.

In this analysis, the channels that fall into the all three regions of Raman gain profile are determined first considering the channels to be equally spaced. Power depletions for all three regions are then determined as follows:

$$D_1 = \frac{PL_e \gamma_p}{3 \times 10^{13} A} \sum_{i=1}^{N_1-1} i\Delta v \qquad (3.4)$$

$$D_2 = \frac{PL_e \gamma_p}{2A} \sum_{i=N_1}^{N_2-1} (-6.087 \times 10^{-13} i\Delta v + 10.06382) \qquad (3.5)$$

$$D_3 = \frac{PL_e a\gamma_p}{2A} \exp\left(\frac{x_0}{b}\right) \sum_{i=N_2}^{N-1} \exp\left(\frac{-i\Delta v}{b}\right) \qquad (3.6)$$

The overall depletion is obtained by adding the depletions of all three regions

$$D = D_1 + D_2 + D_3 \tag{3.7}$$

3.4 Performance Analysis

The power penalty suffered by the system due to SRS crosstalk is given by (2.5). If we require a power penalty X=1 dB, using (2.5), and (3.4) through (3.7) the maximum allowable transmitter power is found to be,

$$P = \frac{0.20567}{Y} \tag{3.8}$$

where

$$Y = \frac{L_e \gamma_p}{2A} \left[\frac{2}{3 \times 10^{13}} \sum_{i=1}^{N_1-1} i\Delta v + \sum_{i=N_1}^{N_2-1} (-5.1999 \times 10^{-13} i\Delta v + 8.8) + \exp\left(\frac{x_0}{b}\right) \sum_{i=N_2}^{N-1} \exp\left(\frac{-i\Delta v}{b}\right) \right]$$

The penalty for a given number of channels can be found by computing probability of error curves and determining the difference in launched power for a given bit error rate (BER) which is discussed in the next chapter.

3.5 Discussions on Results

Fig. 3.1 shows the experimentally found Raman gain profile by the dashed line. The triangular approximation of [Chraplyvy, 1984] is shown by the blue curve, which signifies that only M =$1.5 \times 10^{13}/\Delta v$ number of channels contribute to the depletion of the

shortest-wavelength channel. The red curve shows proposed model of this work, which cares for the Raman gain beyond 15 THz spacing between channels. Now as the whole range of channel spacing is included in the model for the Raman gain so there is no need to make any assumption in calculating the power depletion. Rather the power depletion due to channels from the three regions of the Raman gain can be determined individually and then the total power depletion can be found by adding these contributions. Thus the analytical results are expected to be more accurate and generalised.

Fig. 3.2 shows the estimated power depletion as a function of the number of channels. The system parameters are chosen to be as follows: the fiber loss coefficient, $\alpha = 0.25$ dB/km, $A_{eff} = 5 \times 10^{-7}$ cm^2, $\gamma_p = 6 \times 10^{-12}$ cm/ W ^{2}, launched Power = 1 mW, channel separation, $\Delta\lambda = 10$ nm ($\Delta v = 1.3 \times 10^{12}$ Hz at 1.5 μm). The green curve shows the depletion found in [Chraplyvy, 1984] and the solid line shows the depletion found in this analysis. It is obvious that in both the cases there is a sharp rise in depletion with the increase in number of channels within the linear regime of Raman gains profile. The value of depletion then saturates. However, it is noticed that a significant increase in depletion is found due to the regime beyond 15 THz spacing between channels by using the improved model of the Raman gain profile. The correction in the power depletion due to the region 2 and region 3 of the Raman gain profile are also shown in this figure.

Figure 3.3 shows the gain of different channels versus fiber length of a 41-channel system considering the effect of SRS. Channel 1 is the shortest wavelength channel and suffers the worst depletion. Channel 41 is the longest wavelength channel whose power is
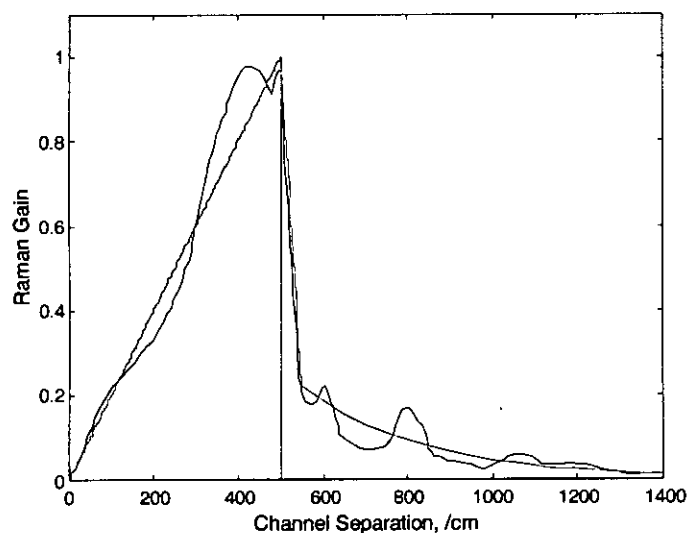
Fig. 3.1. Experimental Raman gain profile (dashed curve), approximation used in [Chraplyvy, 1984] (blue curve) and approximation used in our calculation (red curve).
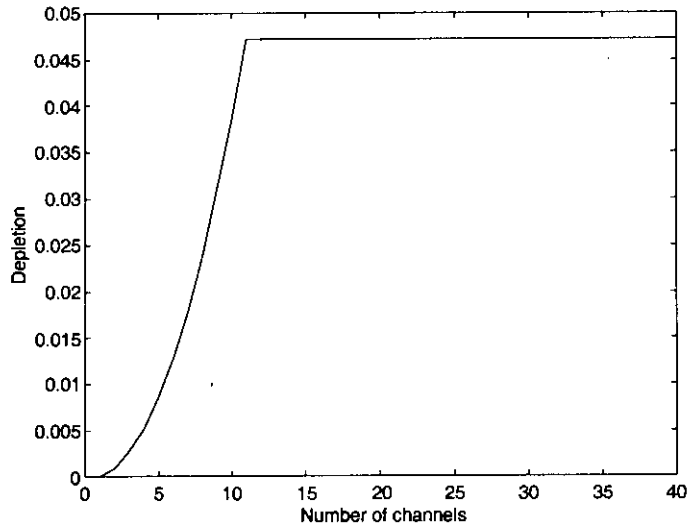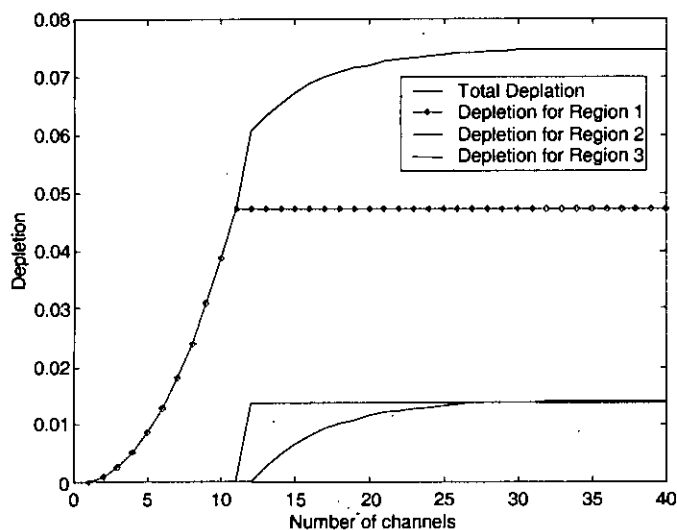

Fig. 3.2 Overall and individual depletion profile as a function of number of channels for typical system parameters, $\alpha = 0.25$ dB/km, $A_{eff} = 5$ x 10^{-7} cm^2, $\gamma_p \sim 6$ x 10^{-12} cm/ W ^{2}, launched power= 1 mW, channel separation, $\Delta\lambda \sim 10$ nm ($\Delta v \sim 1.3$ x 10^{12} Hz at 1.5 μm).
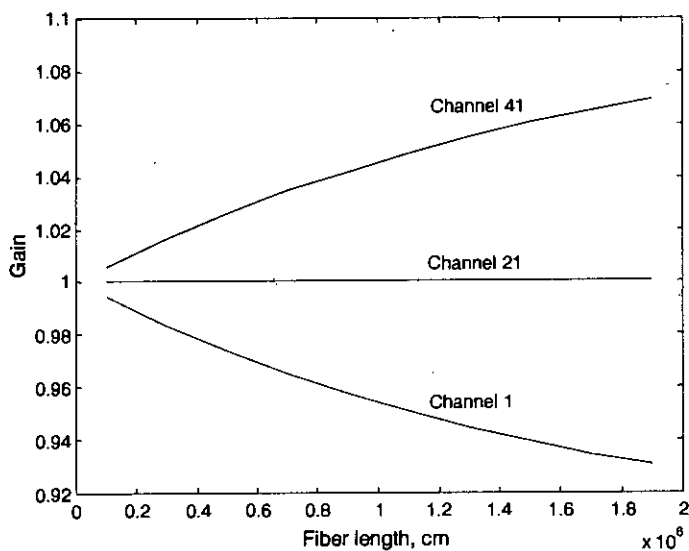
Fig. 3.3: Gain versus fiber length of 41-channel system considering the effect of SRS.

Fig. 3.4: Power penalty for different input power as a function of number of channels using typical system parameters, effective length = 16 km, effective core area, A_{eff} = 5 x 10^{-7} cm^2, $\gamma_p \sim 6$ x 10^{-12} cm/ W^2, launched Power = 1 mW, channel separation, $\Delta\lambda \sim 10$ nm ($\Delta v \sim 1.3$ x 10^{12} Hz at 1.5 μm).

number of channel VS power penalty curve for differnt value of leff
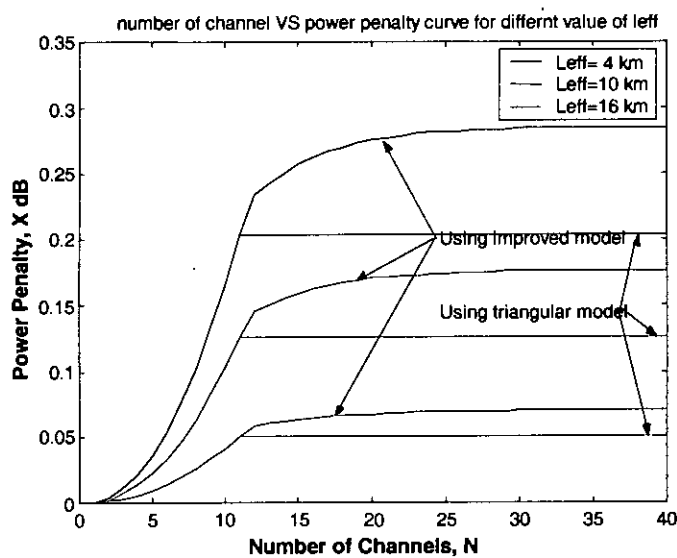
Fig. 3.5: Power penalty for different effective length as a function of number of channels using typical system parameters, $\alpha = 0.25$ dB/km, $A_{eff} = 5$ x 10^{-7} cm^2, $\gamma_p \sim 6$ x 10^{-12} cm/ W^2, launched power = 1 mW, channel separation, $\Delta\lambda \sim 10$ nm ($\Delta v \sim 1.3$ x 10^{12} Hz at 1.5 μm).

Fig. 3.6: Launched power for different effective length as a function of number of channels for a given penalty of 1 dB.

amplified most. Channel 21 is the mid channel and its power remains as it is due to the amplification and depletion obtained from equal number of channels having shorter and longer wavelength than its wavelength respectively.

Fig. 3.4 shows the power penalty suffered by the shortest-wavelength channel due to the SRS effect arising from all the channels in the system. As the number of channels increases, the depletion increases causing more power penalty for a WDM system. The penalty also increases with the power input to the system. Fig. 3.5 shows the power penalty for different effective lengths of the fiber. It is noted that the power penalty increases as the fiber effective length is increased. All these are because of the increasing amount of crosstalk due to the SRS effect.

Now if the system design requires the power penalty to be within a limit, say 1 dB, we get a maximum allowable power for a given value of the effective length and the number of channels. Fig. 3.6 shows the launched power limitations for different fiber effective lengths as a function of the number of channels. It is observed that the allowable input power decreases with the number of channels and also with the fiber length. Thus the maximum input power for a given system can be efficiently estimated from the analysis.

3.6 Conclusion

An improved solution to the evaluation problem of stimulated Raman crosstalk in a WDM fiber optic communication system is presented. The proposed model for the Raman gain

spectrum provides a better and more accurate estimation of the power depletion compared to previous estimates of [Chraplyvy, 1984]. A generalized and more accurate expression for depletion is obtained and is used efficiently for performance calculation. Using these results, the system limitations for a given penalty are found more accurately. The results can be efficiently used for the design of a wideband WDM system.

Chapter 4

STATISTICAL ANALYSIS OF RAMAN

CROSSTALK

4.1 Introduction

To study the stimulated Raman scattering (SRS) induced performance degradation in a wavelength division multiplexed (WDM) system, the probability density function (pdf) of SRS induced crosstalk is essential. The pdf of Raman crosstalk can be well approximated by lognormal distribution, especially in the highly dispersive fiber or with large number of WDM channels. Lognormal distribution in the linear scale is the same as Gaussian distribution in decibel scale. When constant gain or loss is equalized, crosstalk ratio, power penalty, and power limit depend only on the crosstalk variance. Therefore, both power penalty and power limit induced by Raman crosstalk can be evaluated. Since depletion is a random variable, the bit error rate (BER) can be obtained by conditioning on the value of depletion [Marcuse, 1990].

In this chapter, a simplified theoretical treatment for BER and power penalty calculation is provided, where the approximation model for the Raman gain spectrum developed in Chapter 3 is used and the modulation statistics is taken into account. From the BER

curves power penalty is computed. Finally the system limitations for maximum penalty of 1 dB are estimated.

4.2 System Description

An intensity-modulated direct-detection (IM/DD) WDM system with N equally spaced channel is considered. It is assumed that the noise introduced by the optical preamplifier at the receiver determines the system performance. The effect of dispersion is neglected, both assuming no pulse shape distortion and assuming that the signals in all channels propagate at the same speed through the whole fiber. All nonlinear effects other than SRS are also neglected. Finally ZEROS and ONES are assumed to be equally likely, and bits transmitted on different channels are assumed to be independent.

A direct detection receiver essentially consists of the photodetector and plus an amplifier with possibly additional signal processing circuits. Therefore the receiver initially converts the optical signal incident on the detector into an electrical signal, which is then amplified before further processing to extract the information originally carried by the optical signal.

The conditions for coherent detection are not met in IM/DD optical fiber systems. Thus heterodyne and homodyne detection, which is very sensitive techniques and provides excellent rejection of adjacent channels, is not used, as the optical signal arriving at the receiver tends to be incoherent. In practice vast majority of optical communication

systems use incoherent or direct detection in which the variation of optical power level is monitored and no information in phase or frequency content of the signal.

There are three main types of noise due to spontaneous fluctuation in optical fiber communication systems,

1)   Thermal noise introduced by the circuitry following the detector.

2)   Dark current noise due to small leakage current in the photodetector.

3)   Quantum noise produced in the process of creation of an electron-hole pair resulting from the absorption of a photon.

4.3 Theoretical Analysis

The fractional power lost D by the shortest wavelength channel can be expressed in dB by

$$D[dB] = K \begin{bmatrix} \sum_{i=2}^{N_1} \frac{(i-1)m_i}{1.5 \times 10^{13}} + \sum_{i=N_1+1}^{N_2} \left(\frac{8.8}{\Delta v} - 5.199 \times 10^{-13} i \right) m_i \\ + \sum_{i=N_2+1}^{N} a \exp \left(\frac{x_0 - i\Delta v}{b} \right) m_i \end{bmatrix} \qquad (4.1)$$

where $K = \dfrac{PL_e \gamma_p \Delta v}{2A} 10 \log_{10} e$ and P is the peak power transmitted per channel, γ_p is the peak Raman gain coefficient, L_e is the effective fiber length as stated in (2.5), A is the effective core area, m_i is the modulation in the *ith* channel and can assume the value ZERO and ONE with the same probability ½, and Δv is the spacing between channels.

The depletion D is a random variable (RV) due to the randomness of m_i's. The m_i are independent RVs and the central limit theorem [Papoulies, 1995] can be applied to show that D converges to a Gaussian random variable with mean η given the sum of the means η_i of the contributions of each channel,

$$\eta = \sum_{i=1}^{N-1} \eta_i \tag{4.2}$$

variance σ^2 given by the sum of variances σ_i^2 of the contributions of each channel

$$\sigma^2 = \sum_{i=1}^{N-1} \sigma_i^2 \tag{4.3}$$

and pdf of D for Gaussian distribution

$$pdf \ of \ D = \frac{1}{\sigma\sqrt{2\pi}} \exp\left[-\frac{(D-\eta)^2}{2\sigma^2} \right] \tag{4.4}$$

The penalty for a given number of channels can be found by computing probability of error curves and determining the difference in launched power for a given (BER). Since D is a random variable, the probability of error is found by conditioning on the value of D (total probability theorem [Papulies, 1995]) and minimizing the total probability of error to find the best decision threshold. The probability of error is given by

$$P_e = \min_{I_{th}} \left(\frac{1}{2} P_{e|0}(I_{th}) + \frac{1}{2} \sum_D P_{e|1,D}(I_{th}) P_D \right) \tag{4.5}$$

where I_{th} is the threshold level of the decision circuit at the receiver, $P_{e|0}$ is the probability of error when a ZERO has been transmitted, $P_{e|1}$ is the probability of error when a ONE has been transmitted and the bits transmitted on the other channels are such that the channel under consideration is depleted by D. Finally, P_D is the probability of having a depletion D. We append a simplified process similar to [Marcuse, 1990] of

deriving the bit error probability and determining the optimum decision level in appendix D.

4.4 Discussion on Results

Figure 4.1 shows the Gaussian pdf of D for 5 and 10 channels assuming the system parameters are adjusted to get the same maximum depletion of 1 dB in both cases. Gaussian fits the actual pdf in [Forghieri, 1995] very well even for only 10 channels.

Figure 4.2 shows the pdf of D for large values of N (10, 100 and 1000) [Forghieri, 1995] computed with Gaussian approximation. It can be noted that when N increases, the pdf of D tends to be a delta function and crosstalk tends to become deterministic effect since only values of depletion very close to the mean have appreciable probality.

Figure 4.3 shows the pdf of D for 50 channels. System parameters used for calculating the power depletion is kept unaltered. The pdf of maximum depletion is then plotted with Gaussian approximation. The mean is obtained near 0.15, which is close to the half value of maximum depletion.

BER curves have been evaluated using the method described in [Marcuse, 1990] to compute the conditional error probabilities and $P_{e|0}(I_{th})$, $P_{e|1,D}(I_{th})$ which gives more accurate result than the Gaussian approximation of noise at the receiver used in [Forgheiri, 1994]. The procedure is described in Appendix D.
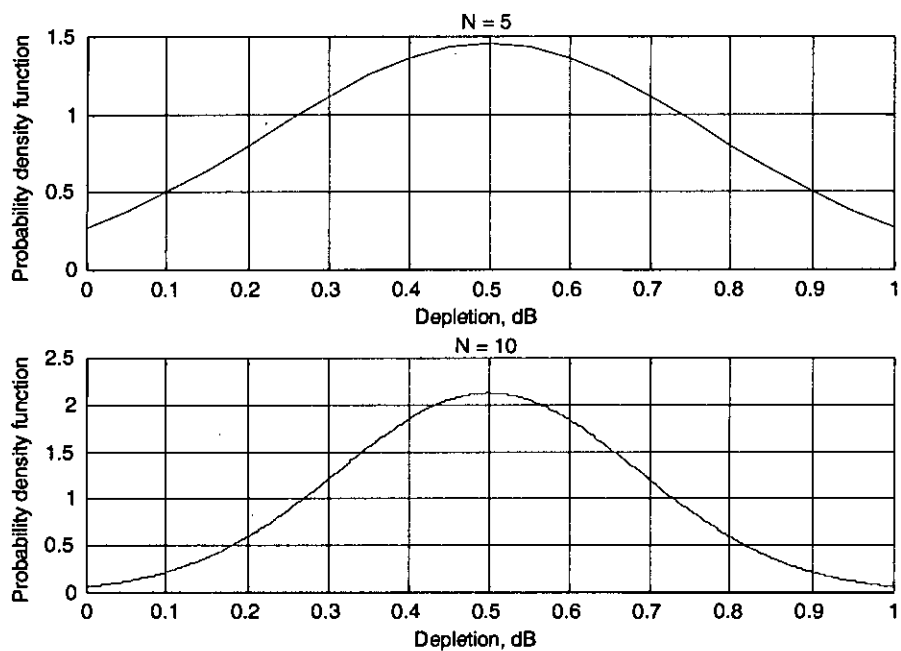
Fig. 4.1: Gaussian fit of the power depletion for 5 and 10 channels and for worst–case depletion of 1 dB.
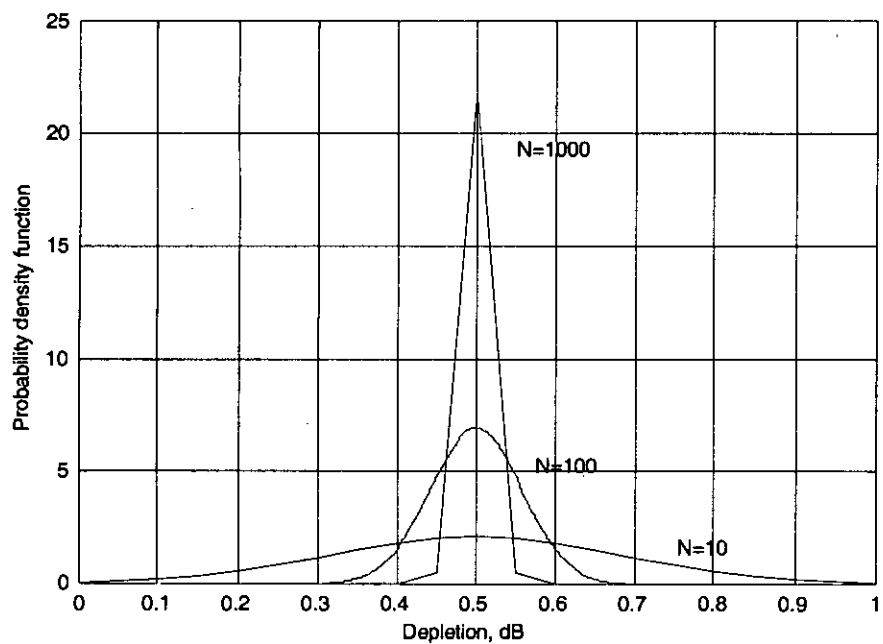
Fig. 4.2: Probability density function of the power depletion for 10, 100 and 1000 channels in the Gaussian approximation for a worst–case depletion of 1 dB.
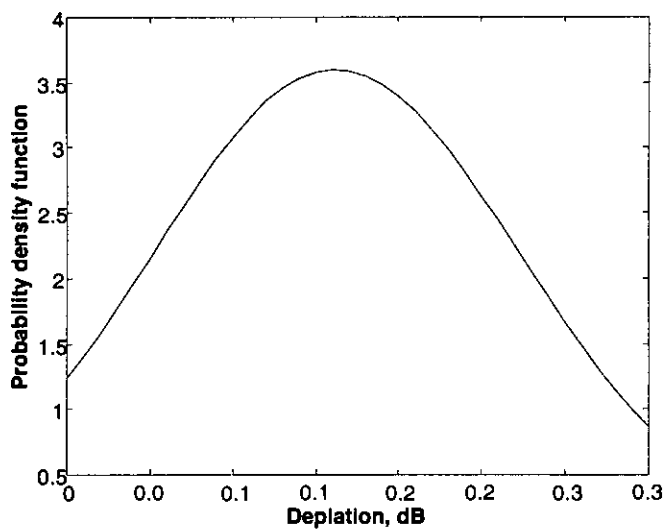
Fig. 4.3: Gaussian pdf of power depletion for 50 channels (in this work).
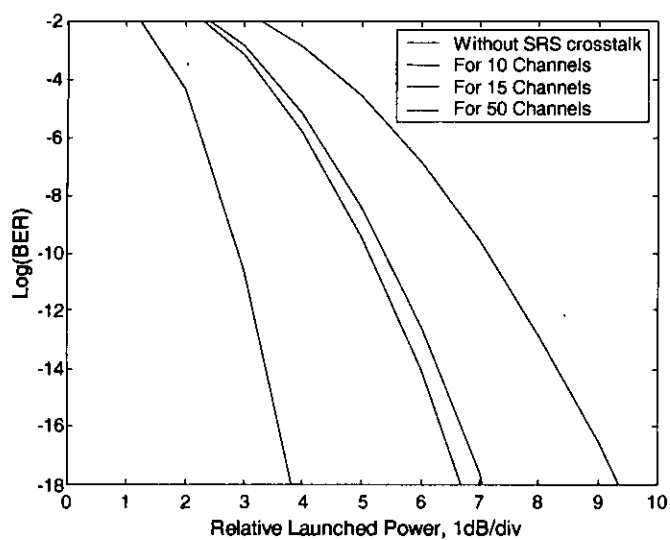
Fig. 4.4: Bit-error-rate curves versus launched power in the channel of interest for 10, 20 and 50 channels. The dashed line is the BER curve for the system without SRS crosstalk.
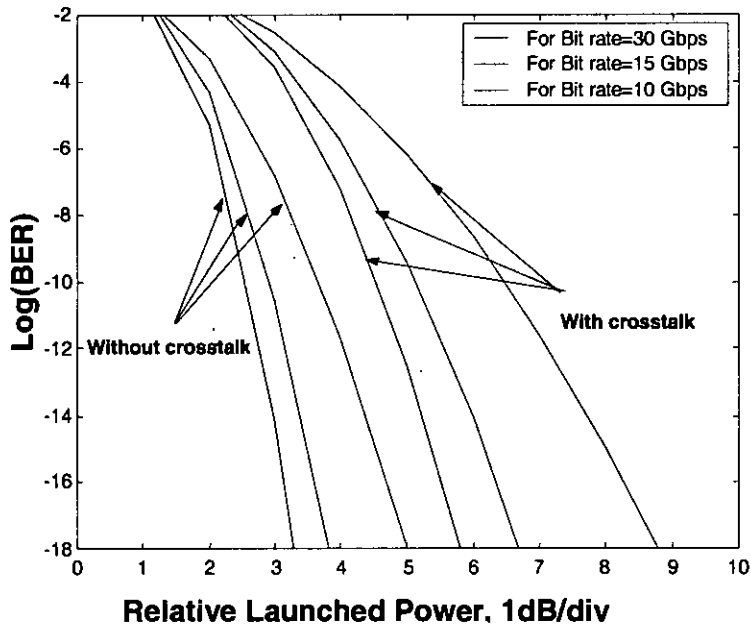
Fig. 4.5: Bit-error-rate curves versus launched power of a 50-channel system for different bit rate. Dashed lines are the BER curves for the system without SRS crosstalk.
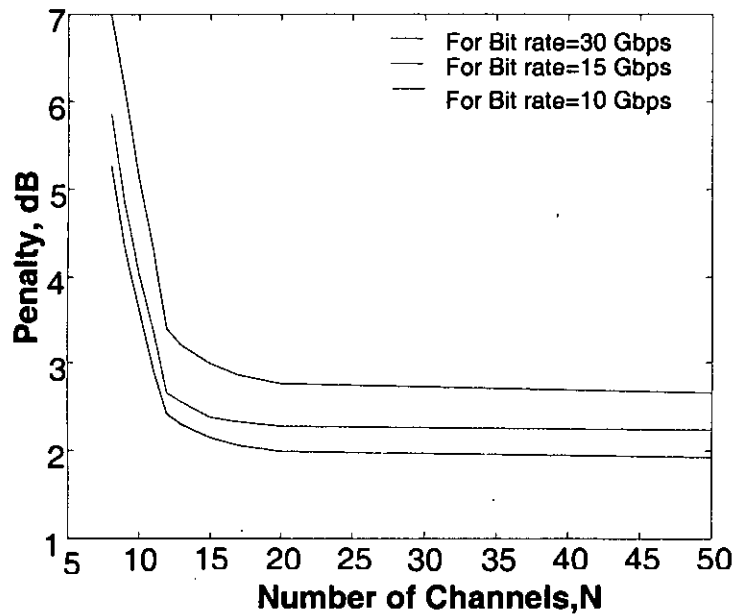
Fig. 4.6: Power penalty versus number of channels for BER = 10^{-9} .

BER have been plotted versus the launched power in the channel of interest, holding other channel's launched power constant to keep the fractional crosstalk constant. Figure 4.4 shows BER curves computed for 10, 15 and 50 channels. The dashed line is the BER curve for the system without SRS crosstalk. However, with the increase of number of channels the curve shifts leftwards when the system is degraded by SRS crosstalk.

An optical filter with bandwidth B is assumed to be used preceding the detector. The bit rate of the system is varied. BER curves are plotted for a 50-channel system in Fig. 4.5. The curves shift leftwards, which imply that the penalty paid by the system is more for higher bit rate.

Power penalty for a given number of channels is determined from the BER curves by determining the difference in launched power for a given BER. It is observed penalty increases more rapidly with increasing N. Figure 4.6 shows the power penalty versus number of channels for different bit rates of 10, 15 and 30 Gbps. It is noted that penalty increases with increased bit rate.

4.5 Conclusion

The probability of error due to SRS crosstalk is evaluated. The probability density function (PDF) of the Raman crosstalk is approximated by a Gaussian distribution. The mean is obtained near the half value of maximum depletion. Therefore the actual penalty is always less than the worst-case penalty. A statistical analysis of the WDM system performance is

developed so to estimate the system bit error rate. BER curves have been evaluated using a more accurate method.

BER curves have been plotted against the launched power in the channel of interest. With the increase of number of channels the curve shifts leftwards when the system is degraded by SRS crosstalk. BER curves are plotted by varying the bit rate. It is observed that the penalty paid by the system is more for higher bit rate.

Power penalty for a given number of channels is determined from the BER curves by determining the difference in launched power for a given BER. The penalty decreases rapidly with increasing N.

Chapter 5

CONCLUSIONS

5.1 Conclusions of this Study

The basic concepts of SRS and its effect on WDM systems are discussed. SRS causes performance degradation by transferring energy from shorter wavelength channel to the larger wavelength channel. The performance evaluation of multichannel system using triangular approximation of Raman gain profile is stated.

An improved model is proposed to approximate the Raman gain profile of silica, which in turn is used to calculate the power depletion of the shortest-wavelength channel due to the SRS effects from all other channels in a wide-band WDM system. With this improved model, the SRS effects from channels at the tail of the Raman gain profile are taken into account.

The channels that fall into the all three regions of Raman gain profile are determined first considering the channels to be equally spaced. Expression for power depletion is then determined. The power penalty suffered by the system due to SRS crosstalk is evaluated. Based on this improved model, the performance analysis technique of a WDM system is modified and generalized.

The probability density function (PDF) of the Raman crosstalk is approximated to be a Gaussian distribution. Thus the probability of error due to SRS crosstalk is evaluated. A statistical analysis of the WDM system performance is developed so to estimate the system bit error rate. Power penalty for a bit error rate 10^{-9} is found which decreases rapidly with increase of number of channels. Finally, the system limitations for a given maximum penalty are quantified. The results are expected to contribute in the design of WDM systems.

5.2 Recommendations for Future Work

In the further research works the non-uniform attenuation characteristics of the fiber can be incorporated in the analysis of SRS to calculate the exact system performance.

Raman crosstalk effects in multimode fiber for a wideband WDM system can be analysed. It can also be extended for different types of fiber.

The effect of group velocity dispersion (GVD) can be incorporated in the analysis.

The analysis can be done assuming that the channels have different input power.

The study can be extended to the field of various crosstalk compensation techniques.

REFERENCES

[1] **Agrawal,** G. P., *Nonlinear Fiber Optics,* 2nd ed. New York: Academic, **1995.**

[2] **Bell,** A. G., "Selenium and the photo phone", *The Electrician,* pp.214, 215,220,221,**1880**

[3] **Boyd,** R. W., *Nonlinear Optics,* Academic press, San Diego, **1992.**

[4] **Cotter,** D. and Hill A. M., "Stimulated Raman crosstalk in optical transmission: effects of group velocity dispersion," *Electron. Lett.,* vol. 20, no. 4, pp. 185-187, **1984.**

[5] **Chraplyvy,** A. R., "Performance degradation due to stimulated Raman scattering wavelength-division-multiplexed optical fibre systems," *Electron. Lett.,* vol. 19, no. 16, pp. 641-643, **1983.**

[6] **Chraplyvy,** A. R., "Optical power limits in multichannel wavelength-division-multiplexed systems due to stimulated Raman scattering," *Electron. Lett.,* vol. 20, no. 2, pp. 58-59, **1984.**

[7] **Chraplyvy,** A. R. and Tkach, R. W. "What is the actual capacity of single-mode fiber in amplified lightwave systems," *IEEE Photon. Technol. Lett.,* vol. 5, pp. 666-668, **1993.**

[8] **Christodulides,** D. N., and Jander, R. B., "Evolution of stimulated Raman crosstalk wavelength division multiplexed systems," *IEEE. Photon. Technol. Lett.,* vol. 8, no. 12, pp. 1722-1724, **1996.**

[9] **Forghieri,** F., Tkach R.W., and Chraplyvy, A. R., "Effect of modulation statistics on Raman crosstalk WDM systems," in *Proc. OAA '94. Breckenridge, CO., paper* FA4, Aug. **1994.**

[10]**Forghieri,** F., Tkach R.W., and Chraplyvy, A. R., "Effect of modulation statistics on Raman crosstalk WDM systems," *IEEE. Photon. Technol. Lett.,* vol. 7, no. 1, pp. 101-103, **1995.**

[11]**Fork,** R. L., Brito Cruz C. H., Becker P. C. and Shank C. V., *Opt. Lett.* vol. 12, pp. 483, **1987.**

[12]**Gomes,** A. S. L., Gouveia-Neto A. S. and Taylor J. R., *Opt Quantum Electron.,* vol. 20, pp. 95, **1988.**

[13]**Gouveia-Neto,** A. S., Gomes A. S. L. and Taylor J. R. *Opt. Quantum Electron.,* vol. 20, pp. 165, **1988**.

[14]**Gower,** J., *Optical communication system,* Prentice-Hall International, Englewood Cliffs, **1993**.

[15]**Ho,** K. P., "Statistical properties of stimulated Raman crosstalk in WDM systems," *J. Lightwave Technol.,* vol. 18, no. 7, pp. 915-921, **2000**.

[16]**Ippen,** E. P. and Stolen R. H., *Appl. Phys. Lett.,* vol 21, pp. 539, **1972**.

[17]**Ippen,** E. P. and Shank C. V. and Gustafson T. K., *Appl. Phys. Lett.,* vol 24, pp. 190, **1974**.

[18]**Islam,** M. N., Mollenauer L. F., Stolen R. H., Simpson J. R. and Shang H. T., *Opt. Lett.,* vol. 12, pp. 814, **1987**.

[19]**Hasegawa,** A. and Tappert F., *Appl. Phys. Lett.,* vol 23, pp. 142, **1973**.

[20]**Kafka,** J. D. and Baer, *Opt. Lett.,* vol. 12, pp. 181, **1987**.

[21]**Keiser,** G., *Optical Fiber Communications,* McGraw-Hill Book Company, New York, **1983**.

[22]**Marcuse,** D., "Derivation of analytical expression for the bit error probability in lightwave systems with optical amplifiers," *J. Lightwave Technol.,* vol. 8, pp. 1816-1823, Dec. **1990**.

[23]**Mollenauer,** L. F., Stolen R. H. and Gordon J. P., *Phys. Rev. Lett,.* vol.45, pp. 1095, **1980**.

[24]**Mollenauer,** L. F. and Stolen R. H., *Opt. Lett.,* vol.9, pp. 13, **1984**.

[25]**Mollenauer,** L. F., Gordon J. P., and Islam M. N., *J. Quantum Ellectron.,* QE-22, pp.157, **1986**.

[26]**Nakatsuka,** H., Grischkowsky D. and Balant A. C. *Phys. Rev. Lett.,* vol. 47, pp. 910, **1981**.

[27]**Nikolaus,** B. and Grischkowsky D., *Appl. Phys. Lett.,* vol. 42, pp. 1, **1983(a)**.

[28]**Nikolaus,** B. and Grischkowsky D., *Appl. Phys. Lett.,* vol. 43, pp. 228, **1983(b)**.

[29]**Norimatsu,** S. and Yamamoto T., "Waveform distortion due to stimulated Raman scattering in wide-band WDM transmission systems," *J. Lightwave Technol.,* vol. 19, no. 2, pp. 159-171, **2001**.

[30]**Poole,** S. B., Payne, D. N., Mears R. J., Fermann M. E. and Laming R. E., *J. Lightwave Technol.,* vol. 4, pp.870, **1986**.

[31]Papoulis, A., *Probability, Random Variables, and Stochastic Processes,* New York: McGraw-Hill, **1991**.

[32]Shanak, C. V., Fork R. L., Yen R., Stolen R. H., and Tomlinson W. J. Shang, *Appl. Phys. Lett.,* vol.40, pp.761, **1982**

[33]Shen, Y. R., *Principles of Nonlinear Optics,* Wiley, New York, **1984**.

[34]Smith, R. G., "Optical power handing capacity of low loss optical fibers as determined by stimulated Raman and Brillouin scattering," *Appl. Opt.,* vol 11, pp. 2489-2494, 1972.

[35]Stolen, R. H., Ippen E. P. and Tynes, A. R., *Appl. Phys. Lett.,* vol 20, pp. 62, **1972**.

[36]Stolen, R. H. and Ippen E. P., "Raman gain in glass optical waveguides," *Appl. Phys. Lett.,* vol 22, pp. 276-278, **1973(a)**.

[37]Stolen, R. H. and Ashkin A., *Appl. Phys. Lett.,* vol 22, pp. 294, **1973(b)**.

[38]Stolen, R. H. Bjorkholm J. E. and Ashkin A., *Appl. Phys. Lett.,* vol 24, pp. 308, **1974**.

[39]Stolen, R. H., *IEEE J Quantum Electron.* QE-11, pp. 100, **1975**.

[40]Stolen, R. H. and Lin C., *Appl. Phys. Rev. Lett.,* vol 45, pp. 1095, **1978**.

[41]Stolen, R. H., "Nonlinearity in fiber transmission," *Proc. IEEE,* vol 68, no. 10, pp.1232-1236, **1980**.

[42]Tariq, S. and Palais J. C., "A computer model of non-dispersion-limited stimulated Raman scattering in optical fiber multiple-channel communications," *J. Lightwave Technol.,* vol. 11, no. 12, pp. 1914-1924, **1993**.

[43]Wang, J., Sun X., and Zhang M., "Effect of group velocity dispersion on stimulated Raman crosstalk in multichannel transmission systems," *IEEE. Photon. Technol. Lett.,* vol. 10, no.4, pp. 540-542, **1998**.

LIST OF PUBLICATIONS

[1] **Mostafa** M. G., Rahman M. M., Ali G. M. H., Alam M. J. and Islam M. N., "Performance evaluation of an optical WDM system including the effect of stimulated Raman scattering," in *Proc.4th ICCIT 2001,* pp. 234-238, 2001.

[2] Islam M. N., **Mostafa** M. G., Rahman M. M., Ali G. M. H., Alam M. J. and Karim M. A., "Limitations on wideband WDM communication systems imposed by stimulated Raman scattering," *Optics Communications*, (submitted).

APPENDIX A

List of Parameters

A_{eff} $= 5 \times 10^{-7} \text{ cm}^2$

L_e $= 16 \text{ km}$

N $= 40$

X $= 1 \text{ dB}$

α $= 0.25 \text{ dB} / \text{Km}$

γ_p $= 6 \times 10^{-12} \text{ cm/W}$

Δv $= 1.3 \times 10^{12} \text{ Hz}$

$\Delta \lambda$ $= 10 \text{ nm}$

APPENDIX B

MATLAB™ Programs Used

1. Program for plotting the actual and our approximated RAMAN gain profile.

```
clear all;
x0(1)=0;                    y0(1)=0;
x0(2)=20.58824;            y0(2)=0.03852;

% ----------------------data used for region 1------------------------

x1(1)=20.58824;            y1(1)= 0.03852
x1(2)=27.38235;            y1(2)= 0.04704
x1(3)=32.94118;            y1(3)= 0.06556
x1(4)=39.11765;            y1(4)= 0.08407
x1(5)=41.17647;            y1(5)= 0.09259
x1(6)=45.29412;            y1(6)= 0.11111
x1(7)=53.52941;            y1(7)= 0.12963
x1(8)=61.76471;            y1(8)= 0.14815
x1(9)=70.0000 ;            y1(9)= 0.16667
x1(10)=82.35294;           y1(10)=0.18519
x1(11)=92.64706;           y1(11)= 0.2037
x1(12)=102.94118;          y1(12)= 0.22222
x1(13)=121.47059;          y1(13)=0.24074
x1(14)=135.88235;          y1(14)=0.25926
x1(15)=154.41176;          y1(15)=0.27778
x1(16)=168.82353;          y1(16)=0.2963
x1(17)=185.29412;          y1(17)=0.31481
x1(18)=199.70588;          y1(18)=0.33333
x1(19)=210;                y1(19)=0.35185
x1(20)=223.38235;          y1(20)=0.37037
x1(21)=228.52941;          y1(21)=0.38889
x1(22)=240.88235;          y1(22)=0.40741
x1(23)=247.05882;          y1(23)=0.42593
x1(24)=257.35294;          y1(24)=0.44444
x1(25)=265.58824;          y1(25)=0.46296
x1(26)=267.64706;          y1(26)=0.48148
x1(27)=274.44118;          y1(27)=0.5
x1(28)=284.11765;          y1(28)=0.51852
x1(29)=287.20588;          y1(29)=0.53704
x1(30)=288.23529;          y1(30)=0.55556
x1(31)=295.02941;          y1(31)=0.57407
x1(32)=298.52941;          y1(32)=0.59259
```

x1(33)=300.58824;   y1(33)=0.61111
x1(34)=307.79412;   y1(34)=0.62963
x1(35)=308.82353;   y1(35)=0.64815
x1(36)=313.97059;   y1(36)=0.66667
x1(37)=315.61765;   y1(37)=0.68519
x1(38)=319.11765;   y1(38)=0.7037
x1(39)=327.35294;   y1(39)=0.72222
x1(40)=329.41176;   y1(40)=0.74074
x1(41)=333.52941;   y1(41)=0.75926
x1(42)=339.70588;   y1(42)=0.77778
x1(43)=346.91176;   y1(43)=0.7963
x1(44)=350;   y1(44)=0.81481
x1(45)=354.11765;   y1(45)=0.83333
x1(46)=360.29412;   y1(46)=0.85185
x1(47)=370.58824;   y1(47)=0.87037
x1(48)=372.64706;   y1(48)=0.88889
x1(49)=380.88235;   y1(49)=0.90741
x1(50)=389.11765;   y1(50)=0.92593
x1(51)=395.29412;   y1(51)=0.94444
x1(52)=407.64706;   y1(52)=0.96296
x1(53)=415.88235;   y1(53)=0.97778
x1(54)=432.35294;   y1(54)=0.97815
x1(55)=445.64706;   y1(55)=0.97222
x1(56)=453.88235;   y1(56)=0.96296
x1(57)=460.94118;   y1(57)=0.94444
x1(58)=465.05882;   y1(58)=0.93519
x1(59)=480.06471;   y1(59)=0.91296
x1(60)=487.58824;   y1(60)=0.94444
x1(61)=495.88235;   y1(61)=0.96296
x1(62)=500.29412;   y1(62)=0.968296

%-----------------------------data used for region 2-------------------------

x2(1)=500.29412;   y2(1)=0.968296
x2(2)=508.41176;   y2(2)=0.83333
x2(3)=510.52941;   y2(3)=0.74074
x2(4)=516.64706;   y2(4)=0.64815
x2(5)=521.76471;   y2(5)=0.55556
x2(6)=526.88235;   y2(6)=0.52365
x2(7)=530.05882;   y2(7)=0.42593
x2(8)=535.29412;   y2(8)=0.35015
x2(9)=544.55882;   y2(9)=0.24074
x2(10)=545.58824;   y2(10)=0.23256
x2(11)=549.70588;   y2(11)=0.2037
x2(12)=557.94118;   y2(12)=0.18519

% --------------------------------data used for region 3--------------------------------

x3(1)=557.94118;   y3(1)=0.18519
x3(2)=576.47059;   y3(2)=0.17593
x3(3)=584.70588;   y3(3)=0.18519
x3(4)=592.94118;   y3(4)=0.2037
x3(5)=597.05882;   y3(5)=0.21481
x3(6)=605.29412;   y3(6)=0.22222
x3(7)=614.55882;   y3(7)=0.2037
x3(8)=617.64706;   y3(8)=0.18519
x3(9)=624.85294;   y3(9)=0.16667
x3(10)=627.94118;   y3(10)=0.14815
x3(11)=636.17647;   y3(11)=0.12963
x3(12)=638.23529;   y3(12)=0.11111
x3(13)=655.73529;   y3(13)=0.09259
x3(14)=669.11765;   y3(14)=0.08333
x3(15)=689.70588;   y3(15)=0.07407
x3(16)=712.35294;   y3(16)=0.07222
x3(17)=728.82353;   y3(17)=0.07407
x3(18)=745.29412;   y3(18)=0.07778
x3(19)=759.70588;   y3(19)=0.09259
x3(20)=765.88235;   y3(20)=0.11111
x3(21)=773.08824;   y3(21)=0.12963
x3(22)=780.29412;   y3(22)=0.14815
x3(23)=785.44118;   y3(23)=0.16481
x3(24)=802.94118;   y3(24)=0.16667
x3(25)=815.29412;   y3(25)=0.1537
x3(26)=823.52941;   y3(26)=0.13889
x3(27)=833.82353;   y3(27)=0.12963
x3(28)=843.08824;   y3(28)=0.11111
x3(29)=848.23529;   y3(29)=0.09259
x3(30)=848.23529;   y3(30)=0.07407
x3(31)=857.5;   y3(31)=0.06111
x3(32)=864.70588;   y3(32)=0.05556
x3(33)=879.11765;   y3(33)=0.05556
x3(34)=895.58824;   y3(34)=0.0463
x3(35)=910;   y3(35)=0.04259
x3(36)=926.47059;   y3(36)=0.03889
x3(37)=947.05882;   y3(37)=0.03519
x3(38)=965.58824;   y3(38)=0.02778
x3(39)=980;   y3(39)=0.02593
x3(40)=1006.76471;   y3(40)=0.03519
x3(41)=1008.82353;   y3(41)=0.03889
x3(42)=1025.29412;   y3(42)=0.0463
x3(43)=1037.64706;   y3(43)=0.05556
x3(44)=1050;   y3(44)=0.05833
x3(45)=1070.58824;   y3(45)=0.05741
x3(46)=1089.11765;   y3(46)=0.0537
x3(47)=1105.58824;   y3(47)=0.04259
x3(48)=1115.88235;   y3(48)=0.03704

```
x3(49)=1132.35294;      y3(49)=0.03519
x3(50)=1152.94118;      y3(50)=0.03426
x3(51)=1167.35294;      y3(51)=0.03704
x3(52)=1182.79412;      y3(52)=0.03889
x3(53)=1194.11765;      y3(53)=0.03704
x3(54)=1214.70588;      y3(54)=0.03519
x3(55)=1235.29412;      y3(55)=0.03333
x3(56)=1255.88235;      y3(56)=0.02222
x3(57)=1276.47059;      y3(57)=0.01852
x3(58)=1297.05882;      y3(58)=0.01481
x3(59)=1317.64706;      y3(59)=0.01296
x3(60)=1338.23529;      y3(60)=0.01278
x3(61)=1358.82353;      y3(61)=0.01204
x3(62)=1379.41176;      y3(62)=0.012
x3(63)=1400;            y3(63)=0.01187


% ---------------------------- Chraplyvy's profile -------------------------------

x4(1)=500;    y4(1)=1.0;
x4(2)=500; y4(2)=0;


% ------------------------------- our approximated profile ------------------------

f=30e9;
gp=1;                %gp=6e-12;

% ------------------------------------region 1 --------------------------------------

p1=1:1:500;
q1=p1*f*gp/1.5e13;
%------------------------------------region 2 --------------------------------------
p2=500:1:550;
q2=((-p2*f/1.9231e12)+8.8)*gp;


% ------------------------------------region 3 --------------------------------------

x0=1.62E13;
A1=.22675;
t1  =8.64655E12;
p3=550:50:1400;
q3= A1*gp*exp(-(p3*f-x0)/t1);

plot(x0,y0,'r.',x1,y1,'r.',x2,y2,'r.',x3,y3,'r.',x4,y4,'--',p1,q1,p2,q2,p3,q3);
axis([0 1400 0 1.1]);
grid on;
```

2. Program for plotting the Overall and individual depletion profile as a function of number of channels.

```
clear all;

%   le = effective length, gama_peak=peak value of raman gain
%   Dep= total fractional power lost by zeroth channel
%   a=effective core area of fibre, p=input power
%   N=channel number

f=30e9;
p=1e-3;
y=1;
ch_spc=1.3e12;        %   channel separation 1.3e12 Hz at 1.5 micro meter

for N=1:1:40
  noc(y)=N ;

% actual equation : d1=(p*le*gama_peak)/(4*a)*((1.5e13-ch_spc)/ch_spc-(1.5e13-
% ch_spc)*(3e13-ch_spc)/(new0*3*ch_spc))
% taking typical value of (le*gama_peak)/a = 19.8 & converting to polynomial

bw=N*ch_spc;
if bw<500*f
  N11=N
  N22=0
  N33=0
elseif bw<550*f
  N11=500*f/ch_spc
  N22=N
  N33=0
elseif bw<1400*f
  N11=500*f/ch_spc
  N22=550*f/ch_spc
  N33=N
else
  N11=500*f/ch_spc
  N22=550*f/ch_spc
  N33=1400*f/ch_spc
end
% --------------------------------------------------region 1 ------------------------------------------
N1=round(N11);        %round to higher nearest integer
if N1>N11
  N1=N1-1;
end
x=2;
rd1(1)=0;

for i=1:1:(N1-1)
  rd1(x)=rd1(x-1)+i*ch_spc/3e13;
```

```
  x=x+1;
end
d1(y)=p*19.8*rd1(x-1)


% -------------------------------------------------region 2 ------------------------------------


N2=round(N22);
if N2>N22
  N2=N2-1;
end

% actual equation : d2=(p*le*gama_peak)/(2*a)*(8.411*(1.5e12-ch_spc)/ch_spc-
(1.5e12-ch_spc)*(40.82e12+ch_spc)/(new0*7.7*ch_spc))
% converting to plynomial

x=2;
rd2(1)=0;
k=8.8;
B=-1.9231e12;

for i=N1:1:(N2-1)
  rd2(x)=rd2(x-1)+(ch_spc*i/B+k)
  x=x+1;
end
d2(y)=p*9.9*rd2(x-1)


% --------------------------------------------------region 3 ------------------------------------

x0=1.62e13;
a=1.45012e-12;
t=6.35105e12;
c=9.9/6e-12;

x=2;
rd3(1)=0;
N3=fix(N33);

for i=N2:1:(N3-1)
  rd3(x)=rd3(x-1)+exp(-(i*ch_spc-x0)/t)
  x=x+1;
end
d3(y)=a*p*c*rd3(x-1)
Dep(y)=d1(y)+d2(y)+d3(y)
y=y+1;
end
dd1=' Total Deplation';
dd2=' Depletion for Region 1';
dd3=' Depletion for Region 2';
dd4=' Depletion for Region 3';
```

```
plot(noc,Dep,'k',noc,d1,'*',noc,d2,'-.',noc,d3,'.')
legend(dd1,dd2,dd3,dd4);
grid on;
title('Depletion vs Number of Channels');
xlabel('Number of channels');
ylabel('Depletion');
```

3. Program for plotting the Launched Power for different effective length as a function of number of channels.

```
clear all;

%   gba= gamma_peak/effective core area of fibre
%   pp= power penalty
%   leff= effective length of fibre

new0=3.75e14;              % in Hz (800 nm)
f=30e9;
pp=1;
z=1;
gba=6e-5/5;
ch_spc=1.3e12;

for leff=4e5:6e5:16e5
y=1;

for N=2:1:40
  switch z,
  case 1
    noc1(y)=N;
  case 2
    noc2(y)=N;
  case 3
    noc3(y)=N;
  end

bw=N*ch_spc;
if bw<500*f
  N11=N
  N22=0
  N33=0
elseif bw<550*f
  N11=500*f/ch_spc
  N22=N
  N33=0
elseif bw<1400*f
  N11=500*f/ch_spc
  N22=550*f/ch_spc
```

```
  N33=N
else
  N11=500*f/ch_spc
  N22=550*f/ch_spc
  N33=1400*f/ch_spc
end
```

```
% ---------------------------------------------------region 1 --------------------------------------

N1=round(N11);   %round to higher nearest integer
if N1>N11
  N1=N1-1;
end
x=2;
rd1(1)=0;

for i=1:1:(N1-1)
  rd1(x)=rd1(x-1)+i*ch_spc/3e13;
  x=x+1;
end
d1(y)=leff*gba*rd1(x-1)
```

```
% ---------------------------------------------------region 2 --------------------------------------

N2=round(N22);
if N2>N22
  N2=N2-1;
end

x=2;
rd2(1)=0;
k=8.8;
B=-1.9231e12;

for i=(N1+1):1:N2
  rd2(x)=rd2(x-1)+(ch_spc*i/B+k);
  x=x+1;
end
d2(y)=leff*gba*0.5*rd2(x-1)
```

```
% ---------------------------------------------------region 3 --------------------------------------

x0=1.62e13;
a=1.45012e-12;
t=6.35105e12;
c=leff*gba*0.5/6e-12;

x=2;
rd3(1)=0;
```

```
N3=fix(N33);

for i=(N2+1):1:N3;
  rd3(x)=rd3(x-1)+exp(-(i*ch_spc-x0)/t)
  x=x+1;
end
d3(y)=a*c*rd3(x-1)
dp=d1(y)+d2(y)+d3(y);
dd=0.1085
    switch z,
    case 1
    ip1(y)=deconv(dd,dp);
    case 2
    ip2(y)=deconv(dd,dp);
    case 3
    ip3(y)=deconv(dd,dp);
    end

y=y+1;
end
z=z+1;
end
dd1=' Leff= 4 km';
dd2=' Leff=10 km';
dd3=' Leff=16 km';

semilogx(noc1,ip1,'-.',noc2,ip2,'.',noc3,ip3,'k');
axis([2 100 0 0.35]);
legend(dd1,dd2,dd3);
grid on;
title('Number of Channel VS Launched Power for Differnt Effective Length');
xlabel('Number of Channels, N');
ylabel('Launched Power, watt');
```

4. Program for plotting the Power Penalty for different effective length as a function of number of Channels.

```
clear all;
f=30e9;
p=1e-3;
z=1;
gba=6e-5/5;,
ch_spc=1.3e12;

for leff=4e5:6e5:16e5
y=1;

for N=1:1:40
```

```
    switch z,
    case 1
      noc1(y)=N;
    case 2
      noc2(y)=N;
    case 3
      noc3(y)=N;
    end

 bw=N*ch_spc;
 if bw<500*f
   N11=N
   N22=0
   N33=0
 elseif bw<550*f
   N11=500*f/ch_spc
   N22=N
   N33=0
 elseif bw<1400*f
   N11=500*f/ch_spc
   N22=550*f/ch_spc
   N33=N
 else
   N11=500*f/ch_spc
   N22=550*f/ch_spc
   N33=1400*f/ch_spc
 end

 % ----------------------------------------------------region 1 ------------------------------------

 N1=round(N11);        %round to higher nearest integer
 if N1>N11
   N1=N1-1;
 end
 x=2;
 rd1(1)=0;

 for i=1:1:(N1-1)
   rd1(x)=rd1(x-1)+i*ch_spc/3e13;
   x=x+1;
 end
 d1(y)=p*leff*gba*rd1(x-1)


 % ----------------------------------------------------region 2 ------------------------------------

 N2=round(N22);
 if N2>N22
   N2=N2-1;
 end
```

```
x=2;
rd2(1)=0;
k=8.8;
B=-1.9231e12;

for i=N1:1:(N2-1)
   rd2(x)=rd2(x-1)+(ch_spc*i/B+k);
   x=x+1;
end
d2(y)=leff*p*gba*0.5*rd2(x-1)


% ----------------------------------------------------region 3 -------------------------------------

x0=1.62e13;
a=1.45012e-12;
t=6.35105e12;
c=leff*gba*0.5/6e-12;

x=2;
rd3(1)=0;
N3=round(N33);

for i=N2:1:(N3-1)
   rd3(x)=rd3(x-1)+exp(-(i*ch_spc-x0)/t)
   x=x+1;
end
d3(y)=a*p*c*rd3(x-1)
dep=d1(y)+d2(y)+d3(y);
dd=0.1085
      switch z,
      case 1
      pp1(y)=       -10*log10(1-dep);
      case 2
      pp2(y)=       -10*log10(1-dep);
      case 3
      pp3(y)=       -10*log10(1-dep);
      end
y=y+1;
end
z=z+1;
end
dd1=' Leff= 4 km';
dd2=' Leff=10 km';
dd3=' Leff=16 km';

plot(noc1,pp1,'-.',noc2,pp2,'.',noc3,pp3,'k');
legend(dd1,dd2,dd3);
grid on;
title('number of channel VS power penalty curve for differnt value of leff');
```

```
xlabel('Number of Channels, N');
ylabel('Power Penalty, X dB');
```

5. Program for plotting the Power Penalty for different Input Power as a function of number of channels.

```
clear all;
f=30e9;
z=1;
gba=6e-5/5;
leff=16e5;
ch_spc=1.3e12;

for p=3:1:5
  ip=10^(-p);
  y=1;
for N=1:1:40
  switch z,
  case 1
    noc1(y)=N;
  case 2
    noc2(y)=N;
  case 3
    noc3(y)=N;
  end

bw=N*ch_spc;
if bw<500*f
  N11=N
  N22=0
  N33=0
elseif bw<550*f
  N11=500*f/ch_spc
  N22=N
  N33=0
elseif bw<1400*f
  N11=500*f/ch_spc
  N22=550*f/ch_spc
  N33=N
else
  N11=500*f/ch_spc
  N22=550*f/ch_spc
  N33=1400*f/ch_spc
end

% ----------------------------------------------------region 1 ------------------------------------

N1=round(N11);        %round to higher nearest integer
```

```
if N1>N11
  N1=N1-1;
end
x=2;
rd1(1)=0;

for i=1:1:(N1-1)
  rd1(x)=rd1(x-1)+i*ch_spc/3e13;
  x=x+1;
end
d1(y)=ip*leff*gba*rd1(x-1)
```

% ---region 2 -------------------------------------

```
N2=round(N22);
if N2>N22
  N2=N2-1;
end
x=2;
rd2(1)=0;
k=8.8;
B=-1.9231e12;

for i=N1:1:(N2-1)
  rd2(x)=rd2(x-1)+(ch_spc*i/B+k);
  x=x+1;
end
d2(y)=ip*leff*gba*0.5*rd2(x-1)
```

% ---region 3 -------------------------------------

```
x0=1.62e13;
a=1.45012e-12;
t=6.35105e12;
c=leff*gba*0.5/6e-12;

x=2;
rd3(1)=0;
N3=round(N33);

for i=N2:1:(N3-1);
  rd3(x)=rd3(x-1)+exp(-(i*ch_spc-x0)/t)
  x=x+1;
end
d3(y)=a*c*ip*rd3(x-1)
dep=d1(y)+d2(y)+d3(y);
    switch z,
    case 1
    pp1(y)=-10*log10(1-dep);
```

```
      case 2
      pp2(y)=-10*log10(1-dep);
      case 3
      pp3(y)=-10*log10(1-dep);
      end
y=y+1;
end
z=z+1;
end
dd1=' L Power= 1 mW';
dd2=' L Power= 0.01 mW';
dd3=' L Power= 0.001 mW';

plot(noc1,pp1,'.',noc2,pp2,'-.',noc3,pp3,'k');
axis([1 40 0 0.35]);
legend(dd1,dd2,dd3);
grid on;
title('Power Penalty VS Number of Channel for Differnt Input Power');
xlabel('Number of Channels, N');
ylabel('Power Penalty, X dB');
```

6. Program for plotting the Gaussian fit of power depletion for 40 channels.

```
clear all;

f=30e9;
p=1e-3;
y=1;

ch_spc=1.3e12;
for N=1:1:40
  noc(y)=N ;
    bw=N*ch_spc;

    if bw<500*f
    N11=N
    N22=0
    N33=0
    elseif bw<550*f
    N11=500*f/ch_spc
    N22=N
    N33=0
    elseif bw<1400*f
    N11=500*f/ch_spc
    N22=550*f/ch_spc
    N33=N
```

```
else
N11=500*f/ch_spc
N22=550*f/ch_spc
N33=1400*f/ch_spc

end
```
%---------------------------Region 1-------------------------%

```
N1=round(N11);   %round to higher nearest integer
if N1>N11
N1=N1-1;
end
N1=round(N11);   %round to higher nearest integer
if N1>N11
N1=N1-1;
end
x=2;
rd1(1)=0;
for i=1:1:(N1-1)
    rd1(x)=rd1(x-1)+i*ch_spc/3e13;
    x=x+1;
end
d1(y)=p*19.8*rd1(x-1)
vr1(y)=(p*19.8*rd1(x-1))^2
```

%---------------------------Region 2-------------------------%

```
N2=round(N22);
if N2>N22
    N2=N2-1;
end

x=2;
rd2(1)=0;
k=8.8;
B=-1.9231e12;
for i=N1:1:(N2-1)
    rd2(x)=rd2(x-1)+(ch_spc*i/B+k)
    x=x+1;

end
d2(y)=p*9.9*rd2(x-1)

vr2(y)=(p*9.9*rd2(x-1))^2
```

%---------------------------Region 3-------------------------%

```
x0=1.62e13;
a=1.45012e-12;
```

```
t=6.35105e12;
c=9.9/6e-12;

x=2;
rd3(1)=0;
N3=fix(N33);

for i=N2:1:(N3-1)
    rd3(x)=rd3(x-1)+exp(-(i*ch_spc-x0)/t)
    x=x+1;
end
d3(y)=a*p*c*rd3(x-1)
vr3(y)=(a*p*c*rd3(x-1))^2
vr(y)=vr1(y)+vr2(y)+vr3(y)
Dep(y)=d1(y)+d2(y)+d3(y)

y=y+1;

end
mean=Dep(y-1)*10*log10(exp(1))*.5
var=vr(y-1)*(10*log10(exp(1))*.5)^2
dd=2*mean
z=1
for ddb=0:.01:1
    db(z)=ddb
    cc=(ddb-mean)^2/(2*var)
    pdf(z)=exp(-cc)/sqrt(2*3.14159*var)
    z=z+1
end

plot(db,pdf,'k')
xlabel('Deplation, dB');
ylabel('Probability density function');
```

7. Program for plotting Bit-error-rate curves versus launched power in the channel of interest for 10, 15 and 50 channels including ER curve for the system without SRS crosstalk.

```
clear all;

f=30e9;
p=1e-3;
ch_spc=1.3e12;

q=1;
```

```
for nn=1:1:3
  if nn==1
    N=10;
  elseif nn==2
    N=15;
  else nn==3
    N=50;
  end
    y=1;

    bw=N*ch_spc;
    if bw<500*f
    N11=N
    N22=0
    N33=0
    elseif bw<550*f
    N11=500*f/ch_spc
    N22=N
    N33=0
    elseif bw<1400*f
    N11=500*f/ch_spc
    N22=550*f/ch_spc
    N33=N
    else
    N11=500*f/ch_spc
    N22=550*f/ch_spc
    N33=1400*f/ch_spc
  end
%--------------------------Region 1------------------------%

    N1=round(N11);   %round to higher nearest integer
    if N1>N11
  N1=N1-1;
    end
    x=2;
    rd1(1)=0;
    for i=1:1:(N1-1)
    rd1(x)=rd1(x-1)+i*ch_spc/3e13;
    x=x+1;
    end
    d1=p*19.8*rd1(x-1)
    vr1=(p*19.8*rd1(x-1))^2

%--------------------------Region 2------------------------%

    N2=round(N22);
    if N2>N22
  N2=N2-1;
    end
```

```
x=2;
rd2(1)=0;
k=8.8;
B=-1.9231e12;
for i=N1:1:(N2-1)
rd2(x)=rd2(x-1)+(ch_spc*i/B+k)

x=x+1;

end
d2=p*9.9*rd2(x-1)

vr2=(p*9.9*rd2(x-1))^2
```

%--------------------------Region 3------------------------%

```
x0=1.62e13;
a=1.45012e-12;
t=6.35105e12;
c=9.9/6e-12;

x=2;
rd3(1)=0;
N3=fix(N33);

for i=N2:1:(N3-1)
rd3(x)=rd3(x-1)+exp(-(i*ch_spc-x0)/t)
x=x+1;
end
d3=a*p*c*rd3(x-1)
vr3=(a*p*c*rd3(x-1))^2
vr=vr1+vr2+vr3
Dep=d1+d2+d3
mean=Dep*10*log10(exp(1))*.5
%mn(q)=mean;
var=vr*(10*log10(exp(1))*.5)^2

de=Dep; %0.37
dedb=10*log10(exp(1))*de;

cc=(dedb-mean)^2/(2*var)
pd=exp(-cc)/sqrt(2*3.14159*var)



M=2;
E0=.6;
z=1;
```

```
  for E1=1:1:10
    EE1(z)=E1;
    s=(E1/E0)^2
        sm=s*dedb;

        c1=(2*sqrt(sm)-sqrt(sm-4));
        c2=sqrt(sm-4);
        c3=M*sm;
        pi=3.14;

        t1=1/sqrt(pi*M*c1);
        t2=(4*sm/(sm-4))^(1/4);
        t3=(1+1/M*(c1-2*c2)/(c1*c2));
        t4=exp(-M*c1^(2)/4);

        pe1Ithd=abs((t1*t2*t3*t4)*pd);
        pe0Ith=1/(factorial(M-1))*((c3/4)^(M-1))*(1+4*(M-1)/c3)*exp(-c3/4);

        br=(.5*(pe0Ith+pe1Ithd));
    switch q,
            case 1
        ber1(z)=log(br);
        case 2
        ber2(z)=log(br);
            case 3
        ber3(z)=log(br);
        end

    z=z+1
    end
q=q+1
end
%---------------------------with out D---------------------------%

for E1=1:1:10
  E(z)=E1;
  s=(E1/E0)^2


sm=s;

c1=(2*sqrt(sm)-sqrt(sm-4));
c2=sqrt(sm-4);
c3=M*sm;
pi=3.14;

t1=1/sqrt(pi*M*c1);
t2=(4*sm/(sm-4))^(1/4);
```

```
t3=(1+1/M*(c1-2*c2)/(c1*c2));
t4=exp(-M*c1^(2)/4);

pe1Ithd=(t1*t2*t3*t4);
pe0Ith=1/(factorial(M-1))*((c3/4)^(M-1))*(1+4*(M-1)/c3)*exp(-c3/4);
br=.5*(pe0Ith+pe1Ithd);
berwd(z)=log(br);

z=z+1;
end




%-----------------------------------------------------------------------

dd1=' Without SRS crosstalk';
dd2=' For 10 Channels';
dd3=' For 15 Channels';
dd4=' For 50 Channels';


plot(E,berwd,'k',EE1,ber1,'r',EE1,ber2,'b',EE1,ber3,'k');
legend(dd1,dd2,dd3,dd4);
AXIS([0 10 -18 -2])

xlabel('Relative Launched Power, 1dB/div');
ylabel('Log(BER)');
```

8. Program for plotting Bit-error-rate curves versus launched power of a 50-channel system for different bit rate. Dashed lines are the BER curves for the system without SRS crosstalk

```
clear all;

f=30e9;
p=1e-3;

ch_spc=1.3e12;

q=1;
for M=1:1:3
  N=50;

    y=1;
    bw=N*ch_spc;
    if bw<500*f
    N11=N
```

```
    N22=0
    N33=0
    elseif bw<550*f
    N11=500*f/ch_spc
    N22=N
    N33=0
    elseif bw<1400*f
    N11=500*f/ch_spc
    N22=550*f/ch_spc
    N33=N
    else
    N11=500*f/ch_spc
    N22=550*f/ch_spc
    N33=1400*f/ch_spc
  end
%---------------------------Region 1------------------------%

    N1=round(N11);   %round to higher nearest integer
    if N1>N11
  N1=N1-1;
    end
    x=2;
    rd1(1)=0;
    for i=1:1:(N1-1)
    rd1(x)=rd1(x-1)+i*ch_spc/3e13;
    x=x+1;
    end
    d1=p*19.8*rd1(x-1)
    vr1=(p*19.8*rd1(x-1))^2

%---------------------------Region 2------------------------%

    N2=round(N22);
    if N2>N22
  N2=N2-1;
    end

% actual equation : d2=(p*le*gama_peak)/(2*a)*(8.411*(1.5e12-ch_spc)/ch_spc-
(1.5e12-ch_spc)*(40.82e12+ch_spc)/(new0*7.7*ch_spc))
% converting to plynomial

    x=2;
    rd2(1)=0;
    k=8.8;
    B=-1.9231e12;
    for i=N1:1:(N2-1)
    rd2(x)=rd2(x-1)+(ch_spc*i/B+k)

    x=x+1;
```

```
    end
    d2=p*9.9*rd2(x-1)

    vr2=(p*9.9*rd2(x-1))^2
```

%----------------------------Region 3------------------------%

```
    x0=1.62e13;
    a=1.45012e-12;
    t=6.35105e12;
    c=9.9/6e-12;

    x=2;
    rd3(1)=0;
    N3=fix(N33);

    for i=N2:1:(N3-1)
    rd3(x)=rd3(x-1)+exp(-(i*ch_spc-x0)/t)
    x=x+1;
    end
    d3=a*p*c*rd3(x-1)
    vr3=(a*p*c*rd3(x-1))^2
    vr=vr1+vr2+vr3
    Dep=d1+d2+d3
    mean=Dep*10*log10(exp(1))*.5
    %mn(q)=mean;
    var=vr*(10*log10(exp(1))*.5)^2

de=Dep; %0.37
dedb=10*log10(exp(1))*de;

cc=(dedb-mean)^2/(2*var)
    pd=exp(-cc)/sqrt(2*3.14159*var)



    E0=.6;
z=1;

for E1=1:1:10
    EE1(z)=E1;
    s=(E1/E0)^2
        sm=s*dedb;

        c1=(2*sqrt(sm)-sqrt(sm-4));
        c2=sqrt(sm-4);
        c3=M*sm;
        pi=3.14;
```

```
        t1=1/sqrt(pi*M*c1);
        t2=(4*sm/(sm-4))^(1/4);
        t3=(1+1/M*(c1-2*c2)/(c1*c2));
        t4=exp(-M*c1^(2)/4);

        pe1Ithd=abs((t1*t2*t3*t4)*pd);
        pe0Ith=1/(factorial(M-1))*((c3/4)^(M-1))*(1+4*(M-1)/c3)*exp(-c3/4);

        br=(.5*(pe0Ith+pe1Ithd));


    switch q,
            case 1
        ber1(z)=log(br);
        case 2
        ber2(z)=log(br);
            case 3
        ber3(z)=log(br);
        end

    z=z+1
    end
q=q+1
end
%---------------------------with out D-------------------------%


l=1
for M=1:1:3
  z=1
  for E1=1:1:10
  E(z)=E1;
  s=(E1/E0)^2



sm=s;

c1=(2*sqrt(sm)-sqrt(sm-4));
c2=sqrt(sm-4);
c3=M*sm;
pi=3.14;

t1=1/sqrt(pi*M*c1);
t2=(4*sm/(sm-4))^(1/4);
t3=(1+1/M*(c1-2*c2)/(c1*c2));
t4=exp(-M*c1^(2)/4);

pe1Ithd=(t1*t2*t3*t4);
pe0Ith=1/(factorial(M-1))*((c3/4)^(M-1))*(1+4*(M-1)/c3)*exp(-c3/4);
```

```
br=.5*(pe0Ith+pe1Ithd);
%berwd(z)=log(br);

    switch l,
          case 1
      berwd1(z)=log(br);
      case 2
      berwd2(z)=log(br);
          case 3
      berwd3(z)=log(br);
      end

z=z+1;
end
l=l+1;
end

%-------------------------------------------------------------------------

dd1=' For M=1';
dd2=' For M=2';
dd3=' For M=3';

plot(EE1,ber1,'r',EE1,ber2,'b',EE1,ber3,'k',E,berwd1,'r',E,berwd2,'b',E,berwd3,'k');
legend(dd1,dd2,dd3);
AXIS([0 10 -18 -2])
xlabel('Relative Launched Power. 1dB/div');
ylabel('Log(BER)');
```

APPENDIX C

Curve Fitting Error

Table 1: Error for the triangular approximation [chraplyvy, 1984].

Channel Separation	Actual Gain	Approximated Gain	% Of error
20.58824	0.03852	0.04118	-6.89637
41.17647	0.09259	0.08235	11.05633
70	0.16667	0.14	16.00168
102.94118	0.22222	0.20588	7.35201
121.47059	0.24074	0.24294	-0.91434
168.82353	0.2963	0.33765	-13.95446
210	0.35185	0.42	-19.36905
257.35294	0.44444	0.51471	-15.80998
288.23529	0.55556	0.57647	-3.76387
300.58824	0.61111	0.60118	1.62549
329.41176	0.74074	0.65882	11.05874
350	0.81481	0.7	14.0904
380.88235	0.90741	0.76176	16.05066
407.64706	0.96296	0.81529	15.33458
432.35294	0.97815	0.86471	11.59782
450.88235	0.96296	0.90176	6.35492
475.58824	0.94444	0.95118	-0.71328
500.29412	0.96296	1.00059	-3.90756

Table 2: Error when the remaining Raman gain profile is assumed to be an exponentially decreasing function.

Channel Separation	Actual Gain	Approximated Gain	% Of error
508.41176	0.83333	0.3061	63.26809
526.88235	0.52365	0.2859	45.40178
535.29412	0.35015	0.27715	20.84716
545.58824	0.23256	0.26681	-14.7271
549.70588	0.2037	0.26278	-29.0037
557.94118	0.18519	0.2549	-37.6448
592.94118	0.2037	0.22398	-9.95619
638.23529	0.11111	0.18946	-70.5184
655.73529	0.09259	0.1776	-91.8125
712.35294	0.07222	0.14407	-99.492
759.70588	0.09259	0.12095	-30.6257
802.94118	0.16667	0.10309	38.14814
857.5	0.06111	0.08427	-37.8935
879.11765	0.05556	0.0778	-40.0241
910	0.04259	0.06941	-62.9665
965.58824	0.02778	0.05652	-103.455
1006.76471	0.03519	0.04854	-37.9438
1050	0.05833	0.04138	29.06721
1105.58824	0.04259	0.03369	20.89109
1152.94118	0.03426	0.02828	17.44272
1214.70588	0.03519	0.02251	36.02568
1255.88235	0.02222	0.01934	12.98335
1317.64706	0.01296	0.01539	-18.7473
1358.82353	0.01204	0.01322	-9.78009
1400	0.01187	0.01135	4.36413

Table 3: Error for the second region (500 cm⁻¹ to 550 cm⁻¹) assuming it to be a linearly decreasing function.

Channel Separation	Actual Gain	Approximated Gain	% Of error
508.41176	0.83333	0.86878	-4.2536
526.88235	0.52365	0.58064	-10.88233
535.29412	0.35015	0.44941	-28.34834
545.58824	0.23256	0.28882	-24.19309
549.70588	0.2037	0.22459	-10.25443

Table 4: Error for the third region (550 cm⁻¹ to 1400 cm⁻¹) assuming it to be an exponentially decreasing function.

Channel Separation	Actual Gain	Approximated Gain	% Of error
557.94118	0.18519	0.21307	-15.05237
592.94118	0.2037	0.1887	7.36327
638.23529	0.11111	0.16126	-45.13454
655.73529	0.09259	0.15176	-63.90433
712.35294	0.07222	0.12469	-72.65699
759.70588	0.09259	0.1058	-14.26809
802.94118	0.16667	0.09106	45.36341
857.5	0.06111	0.07536	-23.31565
879.11765	0.05556	0.06991	-25.83291
910	0.04259	0.06281	-47.47369
965.58824	0.02778	0.05179	-86.43533
1006.76471	0.03519	0.0449	-27.58378
1050	0.05833	0.03864	33.7517
1105.58824	0.04259	0.03186	25.1835
1152.94118	0.03426	0.02704	21.084
1214.70588	0.03519	0.02182	37.98959
1255.88235	0.02222	0.01892	14.86775
1317.64706	0.01296	0.01527	-17.80523
1358.82353	0.01204	0.01323	-9.92522
1400	0.01187	0.01147	3.34432

APPENDIX D

Bit Error Rate Analysis

Optical signal of a logical ONE in the time interval of T of one bit is represented by the complex representation $E_s(t) = E_1 \exp(iw_c t)$, where, ω_c is the angular carrier frequency. E_I has a given constant value for logical ONE and it is zero for a logical ZERO. Added to the signal pulses is amplified spontaneous emission noise $e(t)$, which can be represented as a Fourier series that is also defined only for the time duration T of one bit

$$e(t) = \sum_{v=0}^{\infty} c_v e^{i\omega_v t}$$
(D.1)

with

$$\omega_v = \frac{2\pi}{T}$$
(D.2)

The expansion coefficients c_v of the noise are assumed to be Gaussian random variables with zero mean, $\langle c_v \rangle = 0$, and with a variance σ that is related to the noise power in the frequency band $1/T$ that is occupied by one Fourier component.

Prior to entering the detector, the signal and noise are passed through an optical bandpass filter whose width is sufficient to permit the signal to pass unaltered. Its effect on the noise is to reject all frequencies outside the passband of width B_{opt}, which extends from $v = v_1$ to $v = v_1 + M$ with

$$B_{opt} = \frac{M}{T} \qquad (D.3)$$

Thus the filtered noise can be represented by

$$e(t) = \sum_{v=v_1}^{v_1+M} c_v e^{i\omega_v t} \qquad (D.4)$$

The detector produces an electrical current that is proportional to the absolute square value of the sum of signal plus noise

$$I = K \left| E_s(t) + e(t) \right|^2 \qquad (D.5)$$

To decide whether a logical ONE or a logical ZERO has been received the current is averaged over the time duration of one bit so that the decision is based on the quantity

$$y = \frac{1}{T} \int_0^T I \, dt \qquad (D.6)$$

For computing the probability densities for the random variable y with the case of a logical ZERO, setting $E(t)=0$, we substitute (D.4) into (D.5) and (D.5) into (D.6). The squaring operation indicated in (D.5) into a double summation. However, due to the orthogonality of the functions exp $(i\omega_v t)$ over the domain $0 < t < T$, only the diagonal terms in the sum remain after the integration in (D.6) has been performed. This leads to

$$y = K \sum_{v=v_1}^{v_1+M} \left(c_{rv}^2 + c_{iv}^2 \right) \qquad (D.7)$$

where the absolute square magnitude of the complex expansion coefficients has been expressed as the sum of the squares of their real and imaginary parts.

To reach our goal of deriving an expression for the probability density $W_{c|0}(y)$ for y, we introduce its characteristic function

$$G_{c|0}(\zeta) = \int_0^\infty W_{c|0}(y) e^{i\zeta y} dy \qquad (D.8)$$

The characteristic function is defined as the average value of *exp (iζy)*. This average can be computed by introducing the probability densities for the real and imaginary parts of c appearing in (D.7). Since all of them are independent Gaussian random variables, the characteristic function can be expressed as a 2-m fold integral over products of 2-M Gaussian probability densities. Substituting (D.7) into this multiple integral and realizing that all integrals are actually identical, we obtain readily

$$G_{c|0}(\zeta) = \left\{ \frac{1}{\sqrt{2\pi}\sigma} \int_{-\infty}^\infty \exp\left[-\left(\frac{1}{2\sigma^2} - iK\zeta \right) u^2 \right] du \right\}^{2M} \qquad (D.9)$$

or after performing the integration

$$G_{c|0}(\zeta) = \frac{1}{\left(1 - 2iK\sigma^2\zeta\right)^M} \qquad (D.10)$$

The probability density is now obtained as the inverse of the Fourier integral

$$W_{c|0}(y) = \frac{1}{2\pi} \int_{-\infty}^\infty \frac{e^{-i\zeta y}}{\left(1 - 2iK\sigma^2\zeta\right)^M} d\zeta \qquad (D.11)$$

M integrations by parts convert this integral to the form

$$W_{e|0}(y) = \frac{1}{2\pi(M-1)!}\left(\frac{y}{2K\sigma^2}\right)^{M-1} \cdot \int_{-\infty}^{\infty} \frac{e^{-i\zeta y}}{1-2iK\sigma^2\zeta} d\zeta \qquad (D.12)$$

which can be solved by the residue method

$$W_{e|0}(y) = \left(\frac{1}{2K\sigma^2}\right)^{M} \frac{y^{M-1}}{(M-1)!} e^{-\left(\frac{y}{2K\sigma^2}\right)} \qquad (D.13)$$

If the random fluctuations of the variable y exceed the decision threshold current I_{th}, an error is made. The probability for the occurrence of such an error is

$$P_{e|0}(I_{th}) = \int_{I_{th}}^{\infty} W_{e|0}(y) dy \qquad (D.14)$$

The integral in this expression can be expressed in terms of incomplete gamma function

$$P_{e|0}(I_{th}) = \frac{1}{(M-1)!} \Gamma\left(M, \frac{I_{th}}{2K\sigma^2}\right) \qquad (D.15)$$

A useful and accurate approximation of the incomplete gamma function can be obtained by repeated integrations by parts of the integral in (D.14). Keeping the first two terms of the resulting series yields the desired approximation

$$P_{e|0}(I_{th}) = \frac{1}{(M-1)!}\left(\frac{I_{th}}{2K\sigma^2}\right)^{M-1}\left(1 + \frac{2K\sigma^2(M-1)}{I_{th}}\right) e^{-\left(\frac{I_{th}}{2K\sigma^2}\right)} \qquad (D.16)$$

Expression (D.13) for the probability density can be used to compute the average

$$\overline{I_0} = \langle y \rangle = 2K\sigma^2 M \qquad \text{(D.17)}$$

and the variance

$$\sigma_0^2 = M\left(2K\sigma^2\right)^2 = \frac{\overline{I_0^2}}{M} \qquad \text{(D.18)}$$

of y.

Next we compute the probability of error for detecting a logical ONE. Since the signal power is depleted by D due to SRS, we know write (D.5) in the form

$$I_{1D} = K\left[|E_1|^2 D + E_s e^* + E_s^* e + |e|^2\right] \qquad \text{(D.19)}$$

Proceeding in the close analogy to the procedure just outlined for computing $W_{e|0}(y)$, we obtain the following expression for the probability density $W_{e|1,D}(y)$

$$W_{e|1,D}(y) = \frac{1}{2\pi} \int_{-\infty}^{\infty} \frac{\exp\left[-\dfrac{2K^2\sigma^2|E_1|^2 D\zeta^2}{1 - 2iK\sigma^2\zeta}\right]^{-i\zeta y}}{\left(1 - 2iK\sigma^2\zeta\right)^M} e^{i\left(\kappa|E_1|^2 D - y\right)\zeta}\, d\zeta \qquad \text{(D.20)}$$

With the help of (D.17) we use the approximation

$$\left(1 - 2iK\sigma^2\zeta\right)^M \approx e^{-i\overline{I_0}\zeta} \qquad \text{(D.21)}$$

which holds for $MK\sigma^2 <<1$ as well as for $M \to \infty$. With this approximation we can write (D.20) as follows

$$W_{e|1,D}(y) = \frac{1}{2\pi} \int_{-\infty}^{\infty} \exp\left(-\frac{2K^2\sigma^2|E_1|^2 D\zeta^2}{1-2iK\sigma^2\zeta}\right) e^{i(\overline{I_1}D+\overline{I_0}-y)\zeta} d\zeta \qquad (D.22)$$

with the signal current for logical ONEs defined as

$$\overline{I_1} = K|E_1|^2 \qquad (D.23)$$

Using the method of steepest descent we obtain

$$W_{e|1,D}(y) = \frac{1}{2}\sqrt{\frac{M}{\pi I_0}}\left(\frac{\overline{I_1}D}{(y-\overline{I_0})^3}\right)^{1/4} \exp\left[-\frac{M}{I_0}\left(\sqrt{y-\overline{I_0}}-\sqrt{\overline{I_1}D}\right)^2\right] \qquad (D.24)$$

The error probability of mistaking a ONE for a ZERO is given by the expression

$$P_{e|1,D}(I_{th}) = \int_0^{I_{th}} W_{e|1}(y)\, dy \qquad (D.25)$$

When we substitute (D.24) into (D.25) we obtain an integral that does not seem to have a simple solution in terms of known functions. By changing the variable of integration via the substitution

$$x = \left(\sqrt{y-\overline{I_0}}-\sqrt{\overline{I_1}}\right)^2 \qquad (D.26)$$

we obtain

$$P_{e\parallel,D}(I_{th}) = \frac{1}{2}\sqrt{\frac{M}{\pi\,\overline{I_0}}}\left(\overline{I_1}D\right)^{1/4}\int_{x_1}^{x_2}\frac{\exp\left(-\frac{M}{\overline{I_0}}x\right)}{\sqrt{x\left(\overline{I_1}D-\sqrt{x}\right)}}\,dx \qquad (D.27)$$

with the integration limits

$$x_1 = \left(\sqrt{\overline{I_1}D}-\sqrt{\overline{I_{th}}-\overline{I_0}}\right)^2 \qquad (D.28)$$

and

$$x_2 = \left(\sqrt{\overline{I_1}D}-\sqrt{\overline{I_0}}\right)^2 \qquad (D.29)$$

Even though this integral does not seem to have a simple exact solution either, a very good approximation can be obtained by realizing that the integrand contributes primarily near the lower limit $x = x_1$. By expressing the denominator of the integrand by the first two terms of its Taylor series expansion cantered at $x = x_1$, and by letting the upper limit of the resulting integral go to infinity, we obtain the following approximate solution:

$$P_{e\parallel,D}(I_{th}) = \frac{1}{2}\sqrt{\frac{\overline{I_0}}{\pi\,M\,x_1}}\frac{\left(\overline{I_1}D\right)^{1/4}}{I_{th0}}\left[1+\frac{\overline{I_0}}{4M}\frac{\sqrt{x_1}-2\sqrt{I_{th0}}}{x_1\sqrt{I_{th0}}}\right]e^{-\left(M x_1/\overline{I_0}\right)} \quad (D.30)$$

with x_1 given by (D.28) and I_{th} defined as

$$I_{th0} = \overline{I_{th}}-\overline{I_0} \qquad (D.31)$$

If ZEROS and ONES are sent with equal probability one half, the total probability for an error in detecting either a ZERO or a ONE is

$$BER = P_e = \min_{I_{th}} \left(\frac{1}{2} P_{e|0}(I_{th}) + \frac{1}{2} \sum_D P_{e|1,D}(I_{th}) P_D \right) \tag{D.32}$$

It is possible to express the bit error probability in terms of optical signal-to-noise ratio (SNR). To do this, we recall that the detected current $\overline{I_1}$ is proportional to optical signal power of a pulse representing a logical ONE in the absence of noise and depletion. Likewise, the average current $\overline{I_0}$ is proportional to the optical noise power that exists after the optical filter. The optical signal to noise ratio existing after the optical filter can thus be expressed as

$$s = SNR = \frac{\overline{I_1}}{\overline{I_0}} \tag{D.33}$$

Using (D.16), (D.17), (D.30), (D.32) through (D.33), we can finally write

$$BER = \sum_D \frac{\exp(-pTB_{opt}u)}{4\sqrt{\pi pTB_{opt}u}} \left[1 + \frac{\sqrt{sD} - 3\sqrt{s_d - 1}}{4pTB_{opt}u\sqrt{s_d - 1}} \right] \left(\frac{sD}{s_d - 1} \right)^{1/4} \cdot P_D$$
$$+ \frac{(pTB_{opt}s_d)^{TB_{opt}-1}}{2\Gamma(pTB_{opt})} \left[1 + \frac{pTB_{opt} - 1}{pTB_{opt}} \cdot \frac{1}{s_d} \right] \exp(-pTB_{opt} \cdot s_d) \tag{D.34}$$

with the abbreviations

$$s_d = \frac{I_{th}}{I_0} \tag{D.35}$$

and

$$u = \left(\sqrt{sD} - \sqrt{s_d - 1}\right)^2 \tag{D.36}$$

To determine the optimum decision level and plot of BER, the error probability should assume a minimum. Setting the derivative of (D.32) with respect to I_{th} equal to zero yields, with the help of (D.14) and (D.25), the implicit defining equation for I_{th}

$$W_{e|1.D}(I_{th}).P_D = W_{e|0}(I_{th}) \tag{D.37}$$

We take the logarithm of both sides of this equation and after rearranging terms, obtain the following implicit equation for determining $s_d = \frac{I_{th}}{I_0}$

$$s_d = 1 + \frac{1}{4M^2 sD}\left\{MsD - \frac{1}{4}\ln sD - \ln A + (M-1)\ln s_d + \frac{3}{4}\ln(s_d - 1)\right\}^2 \tag{D.38}$$

We have again used

$$M = pTB_{opt} \tag{D.39}$$

and defined the parameter A appearing in (D.38) as

$$A = \frac{\Gamma(M)}{2M^{M-1}\sqrt{\pi M}}$$

(D.40)

Equation (D.38) can be solved by direct iteration. As the signal to noise ratio s approaches to infinity, (D.38) yields the asymptotic solution

$$\frac{s_d}{s} = \frac{1}{4}$$

(D.41)

From (D.34) and (D.38) we can readily write

$$BER = \sum_D \frac{\exp(-pTB_{opt}u)}{4\sqrt{\pi pTB_{opt}u}}\left[1 + \frac{\sqrt{sD} - 3\sqrt{s_d - 1}}{4pTB_{opt}u\sqrt{s_d - 1}}\right]\left(\frac{sD}{s_d - 1}\right)^{1/4} \cdot P_D$$

$$+ \frac{\left(pTB_{opt}s_d\right)^{TB_{opt}-1}}{2\Gamma(pTB_{opt})}\left[1 + \frac{pTB_{opt} - 1}{pTB_{opt}} \cdot \frac{1}{s_d}\right]\exp(-pTB_{opt} \cdot s_d)$$

(D.42)

using equation (D.41) & (D.42) we get

$$BER = \sum_D \frac{\exp\left(-pTB_{opt}\frac{c_1^2}{4}\right)}{2\sqrt{\pi pTB_{opt}c_1^2}}\left[1 + \frac{c_1 - 2c_2}{pTB_{opt}c_1^2c_2}\right]\left(\frac{4sD}{c_2^2}\right)^{1/4} \cdot P_D$$

$$+ \frac{\left(pTB_{opt} \cdot \frac{sD}{4}\right)^{pTB_{opt}-1}}{2\Gamma(pTB_{opt})}\left[1 + \frac{pTB_{opt} - 1}{pTB_{opt}} \cdot \frac{4}{sD}\right]\exp\left(-pTB_{opt} \cdot \frac{sD}{4}\right)$$

(D.43)

where $c_1 = 2\sqrt{sD} - \sqrt{sD - 4}$; $c_2 = \sqrt{sD - 4}$

APPENDIX E

Derivation of Equations

1.   Derivation of Equation (2.3)

For a two-channel (λ_1, λ_2 and $\lambda_1 < \lambda_2$) amplitude modulated WDM system that has a channel (wavelength) spacing such that SRS couples the two channels, if initially two channels have equal optical power injected into the fiber; then the probe channel (λ_2) is intensified and the pump channel (λ_1) is depleted. In a segment of fiber ΔL long assuming scrambled polarization the amplified probe power is:

$$P_2(L + \Delta L) = P_2(L)\exp\left(\frac{\gamma P_1(L)\Delta L}{2A_{eff}}\right) \tag{E.1}$$

where, γ is the SRS gain coefficient and A_{eff} is the effective core area of the fiber. The pump is depleted by:

$$P_1(L + \Delta L) = P_1(L) - \frac{\lambda_1}{\lambda_2}[P_2(L + \Delta L) - P_2(L)] \tag{E.2}$$

For a WDM system having two channels the depletion caused by SRS the shorter wavelength channel is given by

$$D = \frac{\Delta P_1}{P_1(L)}$$

$$= \frac{\frac{\lambda_2}{\lambda_1}(\Delta P_2)}{P_1(L)}$$

$$= \frac{\frac{\lambda_2}{\lambda_1}[P_2(L+\Delta L)-P_2(L)]}{P_1(L)}$$

$$= \frac{\frac{\lambda_2}{\lambda_1}\left[P_2(L)\exp\left(\frac{\gamma P_1(L)\Delta L}{2A}\right)-P_2(L)\right]}{P_1(L)}$$

$$= \frac{\frac{\lambda_2}{\lambda_1}\left[P_2(L)\left\{\exp\left(\frac{\gamma P_1(L)\Delta L}{2A}\right)-1\right\}\right]}{P_1(L)}$$

$$= \frac{\frac{\lambda_2}{\lambda_1}\left[P_2(L)\left\{1+\frac{\gamma P_1(L)\Delta L}{2A}+\left(\frac{\gamma P_1(L)\Delta L}{2A}\right)^2+\wp-1\right\}\right]}{P_1(L)}$$

neglecting the higher terms and considering that equal power has been launched in both the channel, the fractional power loss can be expressed as:

$$D = \frac{\frac{\lambda_2}{\lambda_1}\left[P_2(L)\frac{\gamma P_1(L)\Delta L}{2A}\right]}{P_1(L)}$$

$$D = \frac{\lambda_2}{\lambda_1}\frac{\gamma P_2(L)\Delta L}{2A}$$

Now the above expression can be extended for calculating the fractional power lost by the shortest wavelength channel of an N channel WDM system.

$$D = \sum_{i=1}^{N-1} \frac{\lambda_i}{\lambda_0} \frac{P_i \gamma_i L_e}{2 A_{\text{eff}}}$$

(E.3)

where, P_i is the injected power (watts) in the ith channel, λ_i is the wavelength of ith channel, γ_i is the Raman gain coefficient coupling the ith and the shortest wavelength channel, A_{eff} is the effective core area given by the appropriate overlap integrals [Mittra, 1971], and L_e is the effective fiber length given by:

$$L_e = \left(\frac{1 - e^{-\alpha L}}{\alpha} \right)$$

The actual Raman gain profile of silica is assumed to be a triangular function the peak Raman gain coefficient γ_p occurs at 500 cm^{-1} and assuming there is no Raman interaction at larger spacing. Consequently

$$\gamma_i = \frac{(i\Delta v)\gamma_p}{1.5 \times 10^{13}} \quad , \qquad i\Delta v < 1.5 \times 10^{13} \, \text{Hz}$$

$$\gamma_i = \{(-6.087 \times 10^{-13} \times i\Delta v) + 10.06382\}\gamma_p, \quad 1.5 \times 10^{13} \, Hz \leq i\Delta v \leq 1.65 \times 10^{13} \, \text{Hz}$$

$$\gamma_i = a\gamma_p \exp\left\{ \frac{-(i\Delta v - x_0)}{b} \right\}$$

where, a = 0.22675, x_0 = 1.62×10^{13}, b = 8.64655×10^{12}.

Considering the modulation statistics, the depletion is given by,

$$D = \sum_{i=2}^{N} \frac{P \gamma_i L_{\text{eff}}}{2 A_{\text{eff}}} m_i$$

Depletions in three regions of channel spacing is given by

$$D_1 = \frac{PL_e\gamma_p}{3\times10^{13}A}\sum_{i=1}^{N_1-1} i\Delta v$$

$$D_2 = \frac{PL_e\gamma_p}{2A}\sum_{i=N_1}^{N_2-1}(-6.087\times10^{-13}i\Delta v + 10.06382)$$

$$D_3 = \frac{PL_e a\gamma_p}{2A}\exp\left(\frac{x_0}{b}\right)\sum_{i=N_2}^{N-1}\exp\left(\frac{-i\Delta v}{b}\right)$$

The overall depletion can be found by adding the depletions in three regions

$$D = D_1 + D_2 + D_3$$

Total depletion in dB is given by

$$D[dB] = K\left[\sum_{i=2}^{N_1}\frac{(i-1)m_i}{1.5\times10^{13}} + \sum_{i=N_1+1}^{N_2}\left(\frac{8.8}{\Delta v} - 5.199\times10^{-13}i\right)m_i + \sum_{i=N_2+1}^{N} a\exp\left(\frac{x_0 - i\Delta v}{b}\right)m_i\right]$$

where $K = \frac{PL_e\gamma_p\Delta v}{2A}10\log_{10}e$